Combined lithophile-siderophile isotopic constraints on Hadean processes preserved in ocean island basalt sources

Bradley J. Peters[1,2]*, Andrea Mundl-Petermeier[3,4], Richard W. Carlson[2], Richard J. Walker[4], James M.D. Day[5]

[1]Institute for Geochemistry and Petrology, ETH Zürich, 8092 Zürich, Switzerland

[2]Earth and Planets Laboratory, Carnegie Institution for Science, Washington, DC 20015, USA

[3]Department of Lithospheric Research, University of Vienna, 1090 Vienna, Austria

[4]Department of Geology, University of Maryland, College Park, MD 20742, USA

[5]Scripps Institution of Oceanography, University of California San Diego, La Jolla, CA 92093, USA

*Corresponding author: bradley.peters@erdw.ethz.ch

For submission to: *Geochemistry, Geophysics, Geosystems*

Abstract word count: 239

Main text word count: 8801

Tables: 1

Figures: 8

Supplementary text, tables, and figures accompany this article.

Key Points

- Negative trend between the μ^{142}Nd-μ^{182}W compositions of Réunion OIB and primitive Deccan CFB
- Nd-W isotopic compositions may reflect early magma ocean crystallization and core-mantle interaction
- Stripping of W during subduction can explain the difference in the μ^{142}Nd-μ^{182}W compositions between Réunion OIB and Samoan or Hawaiian OIB

Abstract

Detection of Hadean isotopic signatures within modern ocean island basalts (OIB) has greatly influenced understanding of Earth's earliest history and long-term dynamics. However, a relationship between two isotopic tools for studying early Earth processes, the short-lived ^{146}Sm-^{142}Nd and ^{182}Hf-^{182}W systems, has not been established in this context. The differing chemical behavior of these two isotopic systems means that they are complementary tracers of a range of proposed early Earth events, including core formation, magma ocean processes, and late accretion. There is a negative trend between ^{142}Nd/^{144}Nd and ^{182}W/^{184}W ratios among Réunion OIB that is extended by Deccan continental flood basalts. This finding is contrary to expectations if both systems were affected by silicate differentiation during the lifetime of ^{182}Hf. The observed isotopic compositions are attributed to interaction between magma ocean remnants and Earth's core, coupled with later assimilation of recycled Hadean mafic crust. The effects of this scenario on the long-lived ^{143}Nd-^{176}Hf isotopic systematics mirror classical models invoking mixing of recycled trace-element enriched (sedimentary) and depleted (igneous) domains in OIB mantle sources.

If the core provides a detectible contribution to the tungsten element budget of the silicate Earth, this represents a critical component to planetary-scale tungsten mass balance. A basic model is explored reconciles the W abundance and isotopic composition of the bulk silicate Earth resulting from both late accretion and core-mantle interaction. The veracity of core-mantle interaction as proposed here would have many implications for long-term thermochemical cycling.

Keywords: siderophile elements; early Earth; Earth differentiation; core-mantle interaction; mantle heterogeneity; igneous geochemistry

Plain language summary

Radioactive elements with relatively short half-lives can be used as tools to study the geological processes that took place in the earliest part of Earth's history. Two of these short-lived radioactive tools, the samarium-neodymium and hafnium-tungsten systems, are correlated in the Réunion hotspot source and it is suggested that this results from influences from Earth's metallic core and the preservation of four-billion-year old crust in the deep Earth. The idea that a geochemical fingerprint of Earth's core may make it to the surface has important consequences for broader understanding of Earth's thermal and chemical evolution and possibly changes previous assumptions about the role of late addition of meteorites in establishing Earth's modern tungsten isotopic composition.

1. Introduction

The short-lived ^{146}Sm-^{142}Nd ($t_{1/2}$ = 103 Ma; Friedman et al., 1966) and ^{182}Hf-^{182}W ($t_{1/2}$ = 9 Ma; Vockenhuber et al., 2004) radiogenic isotope systems have been used to probe planetary accretion and differentiation processes occurring within ~70 (^{182}Hf-^{182}W) to ~600 Ma (^{146}Sm-^{142}Nd) following Solar System formation. The elements involved in these two systems have chemical properties that make them useful for studying processes occurring in the early Earth. Tungsten is a moderately siderophile element, but in the absence of metal it behaves as an incompatible trace element in the silicate Earth. Tungsten isotopic compositions different from those of modern rocks ('anomalous' compositions) have been discovered in early Earth rocks and were interpreted to reflect the nature and timing of late accretion (Willbold et al., 2011; Rizo et al., 2016a) as well as early differentiation processes (Touboul et al., 2012; Puchtel et al., 2016a). Despite the large number (>100) of Precambrian rocks now known to possess anomalous ^{182}W/^{184}W, the processes responsible for the development of anomalous ^{182}W/^{184}W signatures remain debated. Similarly, the lithophile ^{146}Sm-^{142}Nd system has been applied in Archean-aged rocks to study Hadean mantle differentiation processes, including magma ocean crystallization (e.g., Caro et al., 2005) and the onset of subduction-type tectonics (e.g., Debaille et al., 2013; Saji et al., 2018).

Some modern ocean island basalts (OIB) are characterized by well-resolved, negative anomalies in ^{182}W/^{184}W relative to laboratory standards and modern mid-ocean ridge basalts (MORB; e.g., Mundl et al., 2017; Rizo et al., 2019) that stand in contrast to the limited variability in ^{142}Nd/^{144}Nd observed in Phanerozoic-aged mantle-derived rocks (e.g., Cipriani et al., 2012; de Leeuw et al., 2017; Horan et al., 2018). Variability in ^{182}W/^{184}W appears to be negatively correlated with ^{3}He/^{4}He within individual OIB systems, but with several distinct slopes among global OIB (Mundl-Petermeier et al., 2020). This observation may provide a link between OIB sources and

the products of early Earth differentiation since high-$^{3}He/^{4}He$ in OIB is commonly taken as evidence for the presence of early-formed, undegassed material in OIB sources. One possible explanation for the presence of negative $^{182}W/^{184}W$ anomalies and high $^{3}He/^{4}He$ in some OIB is the contribution of W and He from core-equilibrated deep mantle domains to mantle plumes that feed hotspot volcanism (Rizo et al., 2019; Mundl-Petermeier et al., 2020).

On the other hand, during silicate differentiation, both Nd and W are more geochemically incompatible than their respective parent elements, Sm and Hf (e.g., Righter & Shearer, 2003; Corgne et al., 2005; Adam & Green, 2006). This means that the Sm-Nd and Hf-W systems should display positive co-variations if they were affected by magmatic differentiation occurring in the silicate Earth before extinction of ^{182}Hf (c.f., Brown et al., 2014). Utilization of these two systems in parallel, therefore, provides a potential means of investigating early processes in the silicate Earth. Despite this apparent complementarity, only one study of modern rocks has reported data for both isotopic systems obtained from the same samples and this study found no obvious correlation (Horan et al., 2018). A robust relationship between the two systems among modern rocks may be unlikely because tectonic recycling and mantle convection may have attenuated anomalous $^{142}Nd/^{144}Nd$ (Jackson et al., 2016) and $^{182}W/^{184}W$ ratios of mantle domains through time, but at different rates. In particular, the $^{142}Nd/^{144}Nd$ ratios of mantle domains may be preferentially overprinted by progressive incorporation of young (<2 Ga), relatively Nd-rich recycled crust into OIB sources, whereas $^{182}W/^{184}W$ may be little influenced by the same process because W can be efficiently removed from subducting oceanic crust (König et al., 2008). By contrast, input of core material into some OIB mantle sources could strongly affect the siderophile isotopic signatures of plume-derived OIB (Rizo et al., 2019; c.f., Brandon et al., 1998) while leaving Nd isotopic signatures unchanged. One or both of these processes may explain why Horan

et al. (2018) observed no correlation between the $^{142}Nd/^{144}Nd$ and $^{182}W/^{184}W$ compositions of OIB from Hawai'i and Samoa.

This contribution investigates the processes that contributed to the Nd-W isotopic compositions of Deccan Traps continental flood basalts (CFB) and Réunion Island OIB, which represent respectively the initial and modern phases of the Réunion hotspot. New and published trace element, $^{143}Nd/^{144}Nd$ and $^{176}Hf/^{177}Hf$ isotopic data are utilized to monitor processes that may have affected the $^{142}Nd/^{144}Nd$ and $^{182}W/^{184}W$ compositions of CFB and OIB, including crustal recycling and assimilation of shallow crustal and depleted mantle components. The Réunion hotspot is the first identified example of an OIB system characterized by significant variability in its $^{142}Nd/^{144}Nd$ composition (Peters et al., 2018). Consequently, it is an ideal location to search for a relationship between Hadean $^{142}Nd/^{144}Nd$ and $^{182}W/^{184}W$ isotopic signatures and explore the relationship of any observed heterogeneity in these systems compared to the long-lived ^{147}Sm-^{143}Nd and ^{176}Lu-^{176}Hf radiogenic isotope systems.

2. Samples & Methods

Basalt and cumulate xenolith samples from the island of La Réunion were examined for their $^{176}Hf/^{177}Hf$ (n = 19) and $^{182}W/^{184}W$ (n = 8) isotopic compositions. The Réunion samples include flows from both Piton des Neiges and Piton de la Fournaise and cover all mapped surficial volcanostratigraphic units (2.1 Ma – present; McDougall et al., 1971; Gillot et al., 1994; **Table 1**). The samples represent a range of geochemical compositions and igneous textures from evolved and nearly aphyric (e.g., sample RU0707, MgO = 7 wt.%) to strongly olivine- and/or clinopyroxene-phyric basaltic lavas (e.g., sample RU0714, MgO = 35 wt.%). Many of these samples have been previously characterized for their $^{3}He/^{4}He$ (Füri et al., 2011), $^{142,143}Nd/^{144}Nd$

(Peters et al., 2018) and $^{187}Os/^{188}Os$ isotopic compositions (Peters et al., 2016). One cumulate dunite xenolith from the Piton Chisny volcanic complex of Piton de la Fournaise was also analysed for its $^{182}W/^{184}W$ ratio in order to determine whether the isotopic compositions of pre-eruptive and post-eruptive igneous rocks are consistent.

Two relatively primitive basalts (MgO = 14-15 wt.%) from the Deccan Traps (*ca.* 65 Ma; Hofmann et al., 2000; Schoene et al., 2015) were also analysed for their $^{142,143}Nd/^{144}Nd$-$^{176}Hf/^{177}Hf$-$^{182}W/^{184}W$ ratios and one basalt from the island of Mauritius (9 Ma-present; Moore et al., 2011) was analysed for its $^{142,143}Nd/^{144}Nd$-$^{176}Hf/^{177}Hf$ isotopic compositions. Because basaltic rocks in these localities are thought to represent earlier manifestations of the Réunion mantle plume (e.g., Duncan et al., 1989), analysis of these samples enables comparison of the short-lived radiogenic isotopic composition of the Réunion hotspot across its lifetime. The Deccan samples have previously been characterized for their $^{3}He/^{4}He$-$^{87}Sr/^{86}Sr$-$^{143}Nd/^{144}Nd$-$^{187}Os/^{188}Os$ (Peters & Day, 2017; Peters et al., 2017) isotopic compositions. The two Deccan samples selected for this study were among those that experienced the least crustal assimilation from the available sample set.

All samples were prepared by sawing with a diamond lap saw and subsequent removal of saw marks with Al_2O_3-paper, followed by crushing and then powdering using alumina ceramic plates and vessels. Care was taken to avoid metal exposure during sample preparation. Sample powders were digested in a ~3:1 HF:HNO_3 solution for >48 hours, repeatedly equilibrated and dried in concentrated HNO_3, then equilibrated in 6M HCl before introduction of the loading acid for the first separation protocol. For Nd and Hf isotopic measurements and for W ID measurements, approximately 100 mg of powder was digested. For W isotopic measurements, the

amount of digested rock powder was determined so that the total W load was 1-1.2 μg, typically resulting in the digestion of 3 to 8 grams of rock powder.

Hafnium was separated from bulk samples using a protocol modified from Münker et al (2001). In brief, high field strength elements including Hf were eluted from the bulk sample fraction on Biorad™ AG50-X8, 200-400 mesh resin in 1M HCl-0.1M HF, then Hf was separated using 100-150 μm Eichrom™ LN-Spec resin from Ti (in citric acid solution) and Zr (in 6M HCl-0.05M HF). Hafnium isotopic compositions were measured on the *Nu Plasma HR* inductively coupled plasma mass spectrometer at the Carnegie Institution for Science, Earth and Planets Laboratory (EPL) and data were reduced using sample-standard bracketing with JMC475 as the bracketing standard.

Tungsten was separated using the method of Peters et al. (2019) in a three-step procedure. First, high field strength elements (HFSE: e.g., Ti, Zr, Ta, Nb) were separated from matrix elements using 1M HCl-0.1M HF on Biorad™ AG50-X8, 100-200 mesh cation exchange resin, analogous to the procedure used for Hf-matrix separation. Then, W was separated using Biorad™ AG1-X8, 100-200 mesh anion exchange resin from Ti and other HFSE (in citric acid solution) and from Hf (in 6M HCl-0.05M HF). Finally, rhenium, tantalum, and other trace elements were removed using 1M HF on Biorad™ AG50-X8, 100-200 mesh cation exchange resin. Measured yields for W were always >80%. Tungsten isotopic compositions were measured on a *Thermo-Fisher Triton* thermal ionization mass spectrometer (TIMS) at the University of Maryland using a multi-static method. In the first measurement line, W isotopic compositions were measured as tungsten trioxides over an integration of 34 seconds. A per-integration oxygen fractionation correction was employed using oxygen isotopic compositions measured with two 10^{12} Ω amplifiers in a second measurement line with an integration lasting 8 seconds. Tungsten isotopic ratios were

also measured in this second line, and all corrected static $^{183}W/^{184}W$ and $^{182}W/^{184}W$ ratios were averaged across a single run. Signals of ^{184}W were typically about 1 volt. All 10^{11} Ω amplifiers were rotated through the analysis routine over 28 blocks of 20 cycles each (i.e., four full rotations and 560 total cycles). Oxygen-corrected $^{182}WO_3/^{184}WO_3$ ratios were then normalized to $^{186}W/^{183}W$ = 0.92767 using the exponential law (c.f., Archer et al., 2017). The average per-session $\mu^{182}W$ precision during this study ($\mu^{182}W = (^{182}W/^{184}W_{sample} \div {}^{182}W/^{184}W_{standard} - 1) * 10^6$) based on repeated measurements of *Alfa Aesar* W standard in each session was ±3.9 ppm (2σ s.d., n = 34) across seven sessions. When normalizing to normalizing to $^{186}W/^{184}W$ = 1.98594, deviations in $^{183}W/^{184}W$ from the standard value (0.467143 ±0.000004) are not observed in sample measurements (average sample $\mu^{183}W$ = 0.7 ±5.1, 2σ s.d., n = 20). Two powder batches of BHVO-2 (#0631 and #1369) analysed over the course of this study (Peters et al., 2019) yielded a mean $\mu^{182}W$ composition of -6.7 ±2.4 (2σ s.d., n = 4; see below for a discussion of statistics reporting), consistent with recent results (e.g., Mundl et al., 2017; Kruijer & Kleine, 2018; Mei et al., 2018; Rizo et al., 2019).

Neodymium was separated from matrix and other rare earth elements utilizing the $NaBrO_3$ method of Garçon et al. (2018). In brief, light rare earth elements were first separated using 6M HCl on Biorad™ AG50-X8, 200-400 mesh cation exchange resin. Then, Ce was separated from Nd using a 10M HNO_3-20 mM $NaBrO_3$ oxidizing solution on 50-100 μm Eichrom™ LN-Spec resin. Following a clean-up column procedure to remove residual Na introduced by the $NaBrO_3$, Nd was again separated from Ce and additionally from La, Pr and Sm on a long-aspect (15-18 cm length x 0.4 cm ID) column containing 20-50 μm Eichrom™ LN-Spec resin using 0.2M HCl. Each column used in the final separation step was re-calibrated for each new batch of 0.2M eluant. Measured yields were typically >80%, except for two digestions of DC1447B: one at EPL (~60%)

and one digestion at ETH performed while the ^{142}Nd separation method was being set up (~30%). The remaining three digestions of this sample had total procedural yields of >80%. There is no observed correlation between yield and stable isotope ratios, despite the possibility of a nuclear field shift effect arising from the use of fine-grained LN-Spec resin (Garçon et al., 2018; *Supplementary Information*). Neodymium isotope compositions were measured on the *Thermo-Fisher Triton* TIMS instruments at EPL and ETH Zürich using a 4-line, multi-dynamic measurement with ^{143}Nd, ^{144}Nd, ^{145}Nd, and ^{146}Nd used sequentially as the center mass. 10^{11} Ω amplifiers were used for all cups and amplifiers were not rotated. Each line was integrated for 8 seconds with a typical intensity of ^{142}Nd ≈ 4-5V. Measured Nd isotopic ratios were normalized to ^{146}Nd/^{144}Nd = 0.7219 using the exponential law. The average per-session μ^{142}Nd precision during this study ($\mu^{142}Nd = (^{142}Nd/^{144}Nd_{sample} \div {}^{142}Nd/^{144}Nd_{standard} - 1) * 10^6$) based on measurements of JNdi-1 Nd standards in each session was ±4.5 ppm (2σ s.d., n = 34) across six sessions. Two separate digestions of BHVO-2 were analysed at ETH during the course of this study and yielded a mean μ^{142}Nd of +3.7 ±3.4 (2σ s.d.).

The internal precision for each run is reported in **Supplementary Tables 1-3**. In **Table 1**, where the weighted average and 2σ weighted standard deviation for each sample are calculated using *Isoplot* (Ludwig, 2003), when n > 1. The per-run precision input into this calculation was the less precise of (1) the 2σ standard error for that run, or (2) the 2σ standard deviation of all standards run in the same analytical session. This approach more conservatively accounts for statistical uncertainty that may arise because of non-ideal or shorter runs (worse 2σ s.e.m. for that run) and/or greater instrument noise across an analytical session (worse 2σ s.d. for standards within that session). When n = 1 for a given sample, the precision reported in **Table 1** is the per-run precision as described above. For samples with n > 1, the appropriateness of this method can be

evaluated using the MSWD of the resulting average, which reports the mean deviation of each sample measurement from the weighted average value. The highest MSWD occurs for sample DC1447B (MSWD = 3.3), which is perhaps predictable because this sample includes measurements from two different mass spectrometers. All other samples have MSWD < 3 for both $\mu^{142}Nd$ and $\mu^{182}W$; many have MSWD < 1. Data from Peters et al. (2018) were re-calculated according to this standard. In many cases, replicate digestions were performed to ensure a better documentation of analytical reproducibility. The $\mu^{142}Nd$ or $\mu^{182}W$ composition of a sample is considered to be anomalous if the range of its precision does not overlap with the long-term average 2σ standard deviation of repeated measurements of laboratory standards, either in the same session ($n = 1$) or across all sessions in which that sample is measured ($n > 1$).

3. Results

Geochemical data are summarized in **Table 1** and reported in full, including all per-barrel precision statistics and stable isotope ratios for TIMS measurements, in **Supplementary Tables 1-3**. Consistent with previous studies of Réunion basalts (e.g., Albarède et al., 1997; Bosch et al., 2008), our samples are characterized by relatively small range of $^{143}Nd/^{144}Nd$ and $^{176}Hf/^{177}Hf$ isotopic signatures (**Figure 1**). The range of $\varepsilon^{176}Hf$ (defined as $(^{176}Hf/^{177}Hf_{sample} / {}^{176}Hf/^{177}Hf_{standard} - 1) * 10^4$) is +8.2 to +9.5 with all compositions lying between hotspots with strong influences from incompatible-element-depleted (higher $\varepsilon^{143}Nd$ and $\varepsilon^{176}Hf$; e.g., Iceland; Stracke et al., 2003; Peate et al., 2010) and -enriched (lower $\varepsilon^{143}Nd$ and $\varepsilon^{176}Hf$; e.g., Samoa; Salters et al., 2011) mantle domains (**Figure 1**). The Deccan samples have lower age-corrected $\varepsilon^{143}Nd$ and $\varepsilon^{176}Hf$ signatures compared to Réunion OIB (+0.2 to +1.2 and -1.0 to +5.5, respectively).

New measurements of μ^{142}Nd in Réunion hotspot volcanic rocks are consistent with previous results (Peters et al., 2018). The Mauritius sample has a μ^{142}Nd composition of +5.6 ±2.1 (*n* = 3), near the upper range of Réunion samples (-7.9 to +6.2, **Figure 2a**; Peters et al., 2018). The two Deccan samples have μ^{142}Nd compositions of +6.6 ±2.5 (*n* = 2) and +11.3 ±1.5 (*n* = 7). Slight variability was observed in the stable isotope compositions of some individual runs, although this did not affect the μ^{142}Nd composition of any run (*Supplementary Information*). The μ^{142}Nd compositions of studied Deccan CFB are consistent with the heterogeneous positive and negative μ^{142}Nd compositions of Deccan basalts reported by Andreasen et al. (2008), although they did not report any samples that were statistically resolved from their standard. The μ^{182}W compositions of Réunion samples range from -2.9 to -9.6 (**Figure 2b**), a range similar to other global OIB (Mundl et al., 2017; Mundl-Petermeier et al., 2019, 2020; Rizo et al., 2019) but do not include μ^{182}W values as low as some reported for Réunion OIB in Rizo et al. (2019). Deccan Traps CFB have μ^{182}W compositions that overlap those of the Réunion OIB (-4.7 to -6.9). Helium and W isotopic data from both locations overlap with observed He-W trends for Samoa and Hawai'i (**Figure 3**; c.f., Mundl et al., 2017), but show only minor variability in their μ^{182}W signatures. Because Réunion OIB have a homogeneous $^{3}He/^{4}He$ signature (*ca.* 12-14 R_A; Füri et al., 2011), it should be expected based on correlations between $^{3}He/^{4}He$ and μ^{182}W in global OIB (Mundl et al., 2017) that the μ^{182}W signature of Réunion OIB is more homogeneous than that of other global hotspots.

The μ^{142}Nd-μ^{182}W composition of Réunion OIB define a negative trend with a slope that is statistically resolved from zero at the 95% confidence level (**Figure 4**). The statistics for this correlation were calculated using *Isoplot* (Ludwig, 2003) with a Model-1 slope of -0.29 ±0.21 (95% c.i.), an MSWD of 1.3 and a probability of fit of 26%. After correcting for crustal assimilation (see *Section 4.2*), the μ^{142}Nd-μ^{182}W compositions of Deccan CFB effectively extend

this trend. The statistics of this combined OIB-CFB correlation (Model-1: MSWD = 1.6 and probability of fit = 14%) are somewhat worse than those for the Réunion OIB alone, which reflects the additional uncertainty introduced by the assimilation correction, however the slope is still resolved from zero (-0.33 ±0.31, 95% c.i.). Although this probability of fit is slightly lower than what *Isoplot* typically recommends for Model-1 fits (≥15%), the Model-2 fit would be inappropriate for these data because it would assume that the uncertainty on both the Réunion data (which represent measured data) and the Deccan data (which represent measured data subjected to a model correction) are the same. Modelled corrections like the one employed in this study for crustal assimilation inherently increase the uncertainty of the resulting data over the measured data because of the assumptions made in the model (see **Table 1** for a comparison). When the correction for crustal assimilation is excluded, the probability of fit for the combined Réunion and Deccan data is substantially higher (35%). However, the slope of the trend in this case is shallower because the uncorrected μ^{142}Nd and μ^{182}W compositions of the Deccan samples are closer to zero, and the slope is correspondingly not resolved from zero at the 95% confidence level. In the case of the Réunion OIB data, the resolved negative slope and low MSWD are consistent with a statistically significant correlation and imply that at least one Réunion mantle source component records a differentiation event that occurred within the lifetime of ^{182}Hf.

The primary statistical limitation on this dataset is its size: a small number of degrees of freedom (6, in the case of the Réunion data alone) in a sample population that is not exhaustive increases the probability that erroneous correlations are discovered. Such a result underscores the need for μ^{142}Nd and μ^{182}W measurements to be undertaken in the same samples, whereas historically different samples have been considered for each isotope system. Importantly, a

statistically significant correlation is not required for the modelling in the discussion to be evaluated as a possible explanation for the history of the Réunion hotspot mantle source.

4. Discussion

4.1 The long-lived radiogenic isotope composition of Réunion-Mauritius OIB

Previous studies have highlighted the relatively homogeneous He-Sr-Nd-Hf-Os-Pb isotopic compositions of Réunion basalts compared to other global OIB that lie towards the center of the 'mantle tetrahedron' (e.g., Albarède et al., 1997; Luais, 2004; Bosch et al., 2008; Füri et al., 2011; Schiano et al., 2012). These characteristics have led to the conclusion that the Réunion mantle source taps a relatively unprocessed mantle domain that was affected by only minor contributions from subducted crust and/or mantle lithosphere (Vlastélic et al., 2006; Bosch et al., 2012; Schiano et al., 2012; Nauret et al., 2019). The new $^{143}Nd/^{144}Nd$-$^{176}Hf/^{177}Hf$ data for Réunion and Mauritius OIB also occupy a narrow range compared to other global hotspots (**Figure 1a**), with the sample from Mauritius having a $^{143}Nd/^{144}Nd$-$^{176}Hf/^{177}Hf$ composition that overlaps with Réunion OIB. Despite this relatively homogeneous isotopic signature, there is a notable trend in the $\varepsilon^{143}Nd$ and $\varepsilon^{176}Hf$ compositions that lies parallel to and above the mantle array (Chauvel et al., 2008), similar to the trends of many other OIB (**Figure 1b**). The $^{143}Nd/^{144}Nd$-$^{176}Hf/^{177}Hf$ mantle array is likely not a unique linear trend, but it functions to qualitatively link the compositions of recycled domains that contribute to OIB mantle sources with bulk depleted mantle with compositions similar to DMM. In Réunion, the lack of a strong trend towards either a DMM or a recycled endmember implies that the geochemical influence of these domains on the Réunion mantle source is relatively minor compared to other global hotspots.

4.2 Post-emplacement alteration and crustal assimilation in Deccan CFB

Continental flood basalts commonly have geochemical compositions that have been strongly modified by crustal assimilation and, to a lesser extent, post-emplacement alteration. Although the two Deccan CFB studied here are relatively fresh picritic lavas, there are still clear differences between their Sr-Nd-Os isotopic compositions and those of Réunion or Mauritius OIB (Peters & Day, 2017) that may have been generated by one or both of these processes. Fluid-mediated flood basalt alteration may progressively leach fluid-mobile elements from proximal basalts or country rock and deliver these elements to other basalts; thus, the net effect of alteration may be to deplete or enrich a CFB sample in fluid-mobile elements. To examine possible effects of post-emplacement alteration on W concentrations, ratios of W to elements that are highly fluid-mobile (e.g., Rb), more moderately fluid-mobile (e.g., U), and fluid-immobile elements (e.g., Th) during crustal weathering are shown in **Figure 5**. Such evaluation is generally not necessary for Nd because it is typically fluid-immobile during flood basalt alteration (e.g., Sheth et al., 2013). In nearly all cases, Deccan basalts show strong depletions in W/Rb, W/U, and W/Th ratios relative to canonical primitive mantle values (McDonough & Sun, 1995) without any apparent trend toward crustal endmembers (Rudnick & Gao, 2003). This implies that fluids that had previously been geochemically influenced by crust did not significantly contribute to the W budget of these samples and thus did not affect their W isotopic compositions.

On the other hand, crustal assimilation has strongly influenced the Sr-Nd-Pb isotopic compositions of many Deccan CFB (e.g., Devey & Lightfoot, 1986; Peng et al., 1994), and this process needs to be considered in order to constrain the Nd-W isotopic compositions of Deccan parental magmas. Assimilation of continental lithospheric mantle (CLM) may also alter the incompatible element budget of ascending CFB magmas, particularly if regional CLM is strongly metasomatized. However, CLM abundances of trace elements are unlikely to be greater than those

of bulk crust, meaning that a model for crustal assimilation would produce a stronger data correction than one for CLM assimilation. Additionally, the effect of CLM assimilation would mimic the effects of crustal assimilation if both crust and CLM are assumed to have μ^{142}Nd and μ^{182}W compositions near zero (c.f., Roth et al., 2014; see *Supplementary Information* for details). By making these assumptions, the following model for crustal assimilation effectively captures the effects of CLM assimilation.

In order to quantitatively account for crustal assimilation effects, the ^{143}Nd/^{144}Nd-^{176}Hf/^{177}Hf isotopic data of the studied Deccan CFB are corrected to an average Réunion OIB composition of ε^{143}Nd = +4.2 and ε^{176}Hf = +8.8. The Deccan parental magma is assumed to have had trace element abundances identical to the Réunion parental magma, which are calculated according to the MgO-trace element correlations present in our samples (Peters et al., 2016; MgO = 13 wt.%, Nd = 18 ppm, Hf = 3.0 ppm, W = 0.18 ppm). This assumption is made based on the shared heritage of Deccan and Réunion lavas inferred from Sr-Nd-Os isotopic systematics (Peters & Day, 2017). Bulk Indian continental crust, through which Deccan CFB erupted, is further assumed to have an average ^{143}Nd/^{144}Nd-^{176}Hf/^{177}Hf composition identical to the Indian Paleoproterozoic metasediments reported in Richards et al. (2005). An initial mixing model was constructed using the trace element abundances calculated by Rudnick & Gao (2003) and then the assumed crustal Nd and Hf abundances were proportionally adjusted in order to produce mixing curves that intersect the studied samples (**Figure 1**; see *Supplementary Table 4* for all model parameters); the assumed crustal W abundance was analogously adjusted for later calculations.

The inferred crustal component is ~16% for sample DC1405 and ~8% for sample DC1447B, similar to the range of inferred upper crust assimilation (ca. 10%) found by Peters & Day (2017) on the basis of the ^{87}Sr/^{86}Sr-^{143}Nd/^{144}Nd compositions of the same samples. The μ^{142}Nd

and $\mu^{182}W$ compositions of the studied samples were then corrected using the same parameters and the assumption that local Neoproterozoic bulk Indian crust has $\mu^{142}Nd = \mu^{182}W = 0$. These calculations resulted in a 1.0 to 1.2 ppm correction for $\mu^{142}Nd$ and a 2.2 to 7.1 ppm correction for $\mu^{182}W$. These results reflect the fact that while the Nd abundances of low-degree mantle partial melts (here 18 ppm) and crust (20 ppm; Rudnick & Gao, 2003) are similar, the W abundances of the two (0.18 and 1 ppm, respectively) are vastly different since W is more incompatible than Nd. Combined with the fact that many Archean crustal terranes have positive $\mu^{182}W$ (**Figure 2**), the correction to the W isotopic compositions of Deccan samples should probably be regarded as a minimum correction. On the other hand, sample DC1447B has a W concentration of 163 ppb, which is similar to the concentrations of Réunion OIB, implying that the effect of crustal assimilation on the W isotopic compositions of some CFB may be relatively small. Further, this model also reveals that because the correction for $\mu^{142}Nd$ is relatively small, CFB may be an untapped source of information about the Nd isotopic compositions of primitive mantle sources, given current standards for $\mu^{142}Nd$ analytical precision.

Because the impact of crustal assimilation on the $\mu^{142}Nd$-$\mu^{182}W$ compositions of Deccan CFB can be quantitatively constrained, this information can be used to assess the geochemical relationship between Deccan CFB and Réunion OIB. Together, both groups of samples define a negative correlation (**Figure 4**), however, in detail there are differences in the compositions of the two localities. Both studied Deccan CFB have negative $\mu^{182}W$ compositions that overlap with those of Réunion OIB. Both Deccan samples also have positive $\mu^{142}Nd$ compositions (defined by the 2σ standard deviation of sample measurements versus that of standard measurements), and sample DC1447B has a positive $\mu^{142}Nd$ anomaly that is the highest among published data for Phanerozoic-aged rocks (see also additional discussion of stable isotope compositions in the

386 *Supplementary Information*). By contrast, Réunion OIB display only minor μ^{142}Nd variability
387 (Peters et al., 2018). The following section explores a model that can account for the origins of
388 these plume components and give rise to the observed μ^{142}Nd-μ^{182}W trend.
389
390 *4.3 Hadean components of the Réunion hotspot mantle source*
391 Archean cratonic rocks preserve both positive and negative μ^{142}Nd compositions (**Figure**
392 **2** and references cited therein), which argues for the existence of at least two isotopically distinct
393 Archean domains resulting from silicate differentiation during the lifetime of ^{146}Sm. The existence
394 of small-scale μ^{142}Nd heterogeneity among Réunion (Peters et al., 2018) and Samoan (Horan et
395 al., 2018) OIB demonstrates that geochemical relics of Hadean silicate differentiation have been
396 at least partially preserved through Earth's history in OIB mantle sources. Many Archean crustal
397 rocks have similar, positive μ^{182}W compositions (**Figure 2**), suggesting that the bulk Archean
398 mantle may have been predominantly characterized by a higher μ^{182}W composition than the
399 present-day mantle. In this context, the negative μ^{182}W compositions found in Schapenburg
400 komatiites (Puchtel et al., 2016) and proximal diamictites (Mundl et al., 2018) may represent a
401 relatively isolated mantle domain. Mantle domains with negative μ^{182}W anomalies may have been
402 formed independently from those with heterogeneous μ^{142}Nd compositions, for example by early
403 Hadean silicate differentiation (e.g., Brown et al., 2014; Puchtel et al., 2016a), heterogeneous
404 assimilation of late-accreted impactors (e.g., Marchi et al., 2018; Archer et al., 2019; Puchtel et
405 al., 2020), or through contributions from Earth's metallic core (e.g., Rizo et al., 2019).
406 Notwithstanding, the existence of coupled, positive (Rizo et al., 2016a) or negative
407 (Puchtel et al., 2016a) μ^{142}Nd-μ^{182}W signatures in some Archean rocks supports the idea that in
408 some cases μ^{142}Nd and μ^{182}W heterogeneity was produced by a common process. The

409 geochemical properties of the ^{146}Sm-^{142}Nd and ^{182}Hf-^{182}W systems predict that such coupled
410 isotopic signatures could be produced during silicate differentiation processes that occurred during
411 the lifetime of ^{182}Hf (Brown et al., 2014). However, the negative μ^{142}Nd-μ^{182}W trend among
412 Réunion OIB and Deccan CFB (**Figure 4**) argues against the idea that heterogeneous μ^{142}Nd and
413 μ^{182}W compositions were formed in a Hadean silicate differentiation event that is preserved in
414 OIB sources, unless the relative incompatibility of parent and daughter elements is different than
415 what is expected from experimental and observational data.

416 One process that may instead lead to a negative correlation between the μ^{142}Nd and μ^{182}W
417 compositions of Réunion hotspot lavas is interaction between a deep mantle domain and the outer
418 core, combined with later additions of Hadean mafic crust. The core has the potential to strongly
419 affect W isotopic compositions in the silicate Earth because of its high W abundance (*ca.* 500 ppb;
420 Arevalo & McDonough, 2008) and highly negative μ^{182}W (*ca.* -220; c.f., Scherstén et al., 2004),
421 whereas the modern BSE has a much lower W abundance of ~13 ppb (Arevalo & McDonough,
422 2008) and $\mu^{182}W \approx 0$. Likewise, Earth's core could affect the He isotopic compositions of mantle
423 domains if it is rich in He and has a high ^{3}He/^{4}He composition (Bouhifd et al., 2020). The overlap
424 of Réunion OIB ^{3}He/^{4}He-μ^{182}W with the trends of other global hotspots interpreted to be affected
425 by core-mantle interaction (Mundl-Petermeier et al., 2020; **Figure 3**) is consistent with the notion
426 that such a process may also have affected the Réunion mantle source. Direct transfer of core metal
427 into deep mantle domains appears to be unlikely in most OIB systems because the core also has
428 high abundances of highly siderophile elements (HSE: Os, Ir, Ru, Pt, Pd, Re). Direct core-mantle
429 exchange would thus lead to high HSE abundances in OIB sources compared to OIB sources that
430 lack a core component. However, the lack of correlations between μ^{182}W and measured or inferred

source abundances of HSE for OIB (Mundl et al., 2017) argues against OIB sources being affected by direct assimilation of core metal into the mantle.

Some models exist to explain how W isotopic equilibration between outer core metal and the lowermost mantle can occur without major consequences for HSE abundances. For example, W equilibration may occur through diffusion between liquid metal and liquid silicate (e.g. Mundl-Petermeier et al., 2020), or between solid metal and solid silicate (Yoshino et al., 2020). However, the latter requires relatively oxidizing conditions at the core-mantle boundary, which contrasts with the predicted slow diffusion rates in the lower mantle at modern oxygen fugacity (Holzapfel et al., 2005). Alternatively, Rizo et al. (2019) suggested that exchange of Si-Mg-Fe oxides between the outer core and a deep mantle silicate liquid could also potentially introduce negative $\mu^{182}W$ compositions into OIB sources without strongly elevating their HSE abundances (c.f., Humayun, 2011). If the equilibrated mantle domain resulting from core-mantle interaction under these circumstances is also interpreted as an early-formed domain with a fractionated (i.e., non-chondritic) lithophile trace element signature, this scenario could explain both the $\mu^{142}Nd$ and $\mu^{182}W$ compositions of Réunion hotspot lavas.

The negative trend of $\mu^{142}Nd$ and $\mu^{182}W$ compositions in Réunion hotspot lavas spans from zero to negative $\mu^{182}W$ compositions but positive to negative $\mu^{142}Nd$ compositions (**Figure 4**), requiring that it was derived from a minimum of two mantle domains: one with positive $\mu^{142}Nd$ and negative $\mu^{182}W$, and one with negative $\mu^{142}Nd$ and zero-to-positive $\mu^{182}W$. Complementary positive and negative $\mu^{142}Nd$ compositions without systematic changes in mantle $\mu^{182}W$ compositions may arise from magma ocean crystallization after the extinction of ^{182}Hf. For example, residual liquids from magma ocean crystallization may be trapped at the base of the mantle (e.g., Labrosse et al., 2007) and would possess enriched incompatible trace element

signatures, including low Sm/Nd ratios. This domain would subsequently evolve a strongly negative μ^{142}Nd composition if it formed within the lifetime of ^{146}Sm. Evidence from seismic tomography indicates that such residual liquids may be present in the roots of modern mantle plumes as ultra-low velocity zones (ULVZ; Yuan & Romanowicz, 2017), although their participation in mantle plume upwelling remains uncertain. Interaction between such a silicate domain and the liquid outer core would likely impart a strongly negative μ^{182}W composition (component 1 in **Figure 6a**). In contrast to magma ocean residual melts, deep-mantle structures such as bridgmanite-enriched ancient mantle structures (BEAMS, Ballmer et al., 2017), formed in the intermediate stages of magma ocean crystallization would possess an incompatible trace-element depleted signature that would evolve a positive μ^{142}Nd composition (component 2). Mixing a small amount of core-equilibrated material into this depleted domain would result in a mixed domain with positive μ^{142}Nd and negative μ^{182}W (component 2a), which is one endmember composition required by the negative correlation. The apparent stability of deep mantle structures in geodynamical models, including BEAMS (Ballmer et al., 2017) and ULVZ (McNamara et al., 2010), means that mantle structures observed by seismic tomography may represent ancient domains that preserve some aspects of their original Hadean geochemical signatures.

One candidate for the second domain in the Réunion source would be a mixture of the enriched and depleted endmembers of a crystallizing magma ocean (i.e., components 1 and 2 in **Figure 6a**). If the W abundances and μ^{182}W compositions of both components were identical, mixing between these two domains would be linear and parallel to the μ^{142}Nd axis. However, this scenario is not consistent with geodynamic models that predict the last liquids of magma ocean crystallization to remain in the deepest mantle (Labrosse et al., 2007), while intermediate solids such as BEAMS would be stable at shallower depths (Ballmer et al., 2017). Further, it is unlikely

that enriched and depleted silicate domains with the same primitive origin would have identical W abundances, although they could have the same $\mu^{182}W$ composition if they formed after the extinction of ^{182}Hf.

A potentially more likely candidate for the second required component would be mafic crust that formed during the lifetime of the ^{146}Sm-^{142}Nd radiogenic system (component 3 in **Figure 6a**). Early mafic crust has been evaluated as an explanation for a variety of trace element and isotopic features of ancient crustal rocks (e.g., Reimink et al., 2014; O'Neil & Carlson, 2017; Rosas & Korenaga, 2018; Carlson et al., 2019). Mafic crust with an incompatible trace-element enriched signature would evolve to negative $\mu^{142}Nd$ compositions and could also have inherited a positive $\mu^{182}W$ composition from a mantle domain similar to the source of Archean tonalite-trondhjemite-granodiorite (TTG) progenitors. Examples of such materials are provided by the mafic supracrustal rocks of the Nuvvuagittuq province (O'Neil et al., 2012; Touboul et al., 2014). Physical mechanisms for returning early crust to the deep mantle without subduction-type tectonics, such as drip-type recycling, have been envisaged (e.g., Moyen & van Hunen, 2012). A small addition of recycled, incompatible trace-element enriched materials is consistent with the conclusions of Nauret et al. (2019) for Piton des Neiges lavas.

Within this framework, a Monte Carlo simulation is used to quantitatively predict the results of a two-stage mixing process for the Réunion source. First, the core-equilibrated silicate domain (component 1a in **Figure 6a**, or 'ULVZ') is mixed with the incompatible element-depleted magma ocean relic (component 2, or 'BEAMS') to produce an array of compositions representing component 2a. The degree of mixing required is small (on average, 0.03% of component 1a) in order to generate a mixed domain with a $\mu^{182}W$ composition of -10 to -30, whereas other hotspots may require slightly greater contributions from the core-equilibrated domain (c.f., Mundl-

Petermeier et al., 2020). The exact amount of mixing depends strongly on the W concentration of the core-equilibrated domain, which is not well-constrained. A relatively small degree of core involvement in the Réunion source is supported by the relatively low HSE abundances inferred for the Réunion mantle source (ca. 30% that of other OIB; Peters et al., 2016). This domain is then mixed with 5-15% recycled mafic crust possessing a modestly negative μ^{142}Nd composition (average: -15) and positive μ^{182}W compositions (median: +15). Mixing curves for this second stage overlap with measured Nd-W isotopic compositions for Réunion hotspot lavas (**Figure 6b**). Notably, the μ^{142}Nd -μ^{182}W trends predicted by the model near the Réunion and Deccan data are relatively flat. Such a finding comports with the overall finding of a negative trend in the data that is most probably resolved from zero (see the end of the *Results* section for detail). A discussion of the handling of uncertainties in this simulation is provided in the *Supplementary Information*.

The same two-stage mixing scenario can also reproduce the ε^{143}Nd and ε^{176}Hf composition of Réunion OIB (**Figure 6c-d**). The mixing lines predicted by the model for ε^{143}Nd and ε^{176}Hf closely mirror those predicted by Chauvel et al. (2008) for interaction between ancient incompatible-element-enriched and -depleted materials. These materials are commonly interpreted as recycled sedimentary and crustal materials, respectively, however our model permits reinterpretation of these recycled domains in a primordial context. Additional, later assimilation of depleted, DMM-like material as the Réunion mantle plume ascends to the surface may elevate the ε^{143}Nd-ε^{176}Hf compositions above the modelled mixing line, as observed in **Figure 6c-d**.

4.4 Preservation of Hadean components in global OIB magmas

The degree of μ^{142}Nd heterogeneity observed in Réunion OIB and Deccan CFB has not yet been observed in other global hotspots. For example, Hawai'i and Samoa OIB show strong μ^{182}W

heterogeneity (Mundl et al., 2017) but only Samoan lavas are characterized by possible minor μ^{142}Nd variability (Horan et al., 2018). Changes in the magnitude of μ^{142}Nd variability may arise if a hotspot source reservoir like that of Réunion is exposed to continuous assimilation of younger material with μ^{142}Nd and μ^{182}W near zero (**Figure 7a**; c.f., Jackson et al., 2016). If this younger material represents recycled oceanic crust and lithosphere, it may additionally contain a low W abundance because W can be efficiently removed by fluids during subduction (König et al., 2008). This would potentially result in preferential overprinting of Hadean μ^{142}Nd compositions while leaving Hadean μ^{182}W compositions relatively unchanged. Similarly, a mantle assimilant with a high intrinsic Nd/W ratio, such as depleted MORB mantle or an ancient, W-depleted reservoir, could also efficiently overprint μ^{142}Nd while leaving μ^{182}W unchanged (c.f., Jackson et al., 2020).

To further examine these possible assimilation effects, the effect of assimilating young material with average μ^{142}Nd and μ^{182}W of 0 and Nd/W ≈ 3000 is modelled. This Nd/W ratio is somewhat higher than what is inferred for modern MORB mantle (Workman & Hart, 2005; Arevalo & McDonough, 2008), however one may expect that the Nd/W ratio of DMM has decreased through time because W is more incompatible than Nd. Time-integrated assimilation of 30-50% of this younger domain into one possessing a Réunion-like μ^{142}Nd-μ^{182}W trend reproduces the μ^{142}Nd-μ^{182}W composition of Hawai'i and Samoa OIB (**Figure 7b**). These proportions would be smaller if the younger domain were more trace-element enriched than modern MORB. The strong ε^{143}Nd-ε^{176}Hf isotopic heterogeneity within Hawaiian and Samoan OIB attests to influence from this younger material (**Figure 1a**). By contrast, the relatively restricted composition of Réunion OIB (**Figure 1b**) corroborates the notion that they escaped substantial assimilation of geologically young material and thus better preserved their original μ^{142}Nd-μ^{182}W trend.

546

547 *4.5 Time-integrated role of core-mantle interaction in the composition of the BSE*

548 Late accretion of materials with broadly chondritic bulk compositions has commonly been
549 proposed as the cause of roughly chondritic relative abundances of HSE and chondritic $^{187}Os/^{188}Os$
550 ratios in the mantle (e.g., Chou, 1978; Walker, 2009). If late accretion was responsible for the
551 majority of the HSE present in the BSE, mass balance requires that at least 0.5 wt.% of Earth's
552 silicate mass was added by this process (e.g., Morgan et al., 2001). Late accretion would similarly
553 replenish the BSE in other siderophile elements, such as W, although at a lesser magnitude (e.g.,
554 Dauphas, 2017). Late accretion is commonly envisioned to have occurred during or after the final
555 stages of core formation in Earth (~30 Ma after Solar System formation). If late accreted materials
556 were initially unevenly distributed in Earth's mantle and not well-mixed in the BSE (so-called
557 'grainy' late accretion), this may provide one explanation for the positive $\mu^{182}W$ present in most
558 Eoarchean rocks (e.g., Willbold et al., 2011). Hence, the timescale over which the isotopic
559 consequences of late accretion would manifest in mantle-derived rocks, leading to a lowering of
560 $\mu^{182}W$, is unclear (e.g., Willbold et al., 2015). This poses some challenges in the interpretation of
561 $\mu^{142}Nd$-$\mu^{182}W$ data.

562 The apparent diminishment in $\mu^{142}Nd$ anomalies of mantle-derived rocks between 3.8 and
563 2.7 Ga (e.g., Rizo et al., 2012; Saji et al., 2018; **Figure 2a**) suggests that the Archean mantle was
564 effective at homogenizing diverse $\mu^{142}Nd$ compositions over approximately 1 Ga timescales.
565 However, over the same time interval the same rock types show a relatively constant range in
566 positive $\mu^{182}W$ compositions, with some notable exceptions (**Figure 2b**). For example, 3-8-3.7 Ga
567 mafic rocks from Isua are characterized by coupled positive $\mu^{142}Nd$ and $\mu^{182}W$ anomalies (Caro et
568 al., 2006; Willbold et al., 2011; Rizo et al., 2016a), whereas 3.3 Ga rocks from the same region

display no μ^{142}Nd anomalies but possess positive μ^{182}W anomalies with magnitudes similar to the 3.8 Ga rocks (Rizo et al., 2016a). Although the existence of positive μ^{182}W anomalies is not ubiquitous among Archean mantle-derived rocks (e.g., Komati: Touboul et al., 2012; Schapenburg: Puchtel et al., 2016a), the persistence of anomalous μ^{182}W compositions into the Neoarchean in any lithology contrasts with the temporal trends hypothesized to exist in the μ^{142}Nd record (e.g., Rizo et al., 2012; Saji et al., 2018). Thus, if the μ^{182}W composition of Earth's Archean mantle was controlled primarily by grainy late accretion, it would require that the timescale of W isotopic homogenization operated independently of the timescale of ^{142}Nd homogenization.

Another possible explanation for the common appearance of positive μ^{182}W anomalies in Archean rocks is that core-mantle interaction, which may have generated the negative μ^{182}W signatures in modern OIB, has lowered the μ^{182}W composition of the BSE from a positive value following late accretion to its current value of zero (c.f., Rizo et al., 2019; Reimink et al., 2020). One attractive aspect of such a hypothesis is that the core-equilibrated silicate domain would likely not become substantially enriched in HSE (Rizo et al., 2019; Mundl-Petermeier et al., 2020), thus allowing the BSE to retain the chondritic relative abundances of these elements imparted on it by late accretion (c.f., Bennett et al., 2002). Thus, core-mantle interaction could have modified the μ^{182}W composition of the bulk mantle while preserving the mantle HSE signatures that represent the classical evidence for late accretion.

To assess the effect of W equilibration at the core-mantle boundary, a simple model was constructed to illustrate the evolution of W abundances and μ^{182}W compositions in the mantle as a consequence of integrated contributions from mantle plumes (**Figure 8**). First, the integrated plume flux into the mantle was estimated according to Davies (1992) for the cross-sectional area of the Hawaiian hotspot swell. It is assumed that, on average, 20% of a plume's mass is directly

returned to the mantle without incorporation into hotspot swells (i.e., that the cross-sections calculated by Davies, 1992, represent 80% of the plume volume), and that the Hawaiian plume represents 10% of the global plume flux at any time in Earth's history. It is approximated that, on average, plumes have $\mu^{182}W$ = -25 and ~35 ppb W before they assimilate ambient mantle material. 5% equilibrium melting of such a plume when D_W = 0.1 yields a primary OIB magma with 280 ppb W, a value similar to Hawaiian and Samoan OIB at 12 wt.% MgO (Mundl et al., 2017). Using these parameters, the integrated effect of mantle plumes on the BSE would be to lower its $\mu^{182}W$ composition by ~13 ppm and raise its W abundance by ~35%. Thus, the model predicts that following late accretion, the BSE had $\mu^{182}W \approx +13$, similar to many Archean rocks (**Figure 2b**). Late accretion is expected to have decreased the $\mu^{182}W$ composition of the BSE by 10-30 ppm, and increased its W abundance by ~8% (Touboul et al., 2015). The combined effects of late accretion and plume additions implies that the BSE had $\mu^{182}W \approx +23$ to +43 following core formation, a range that overlaps the $\mu^{182}W$ compositions of lunar basalts (Touboul et al., 2015; Kruijer et al., 2015). Lunar basalts may not be a direct proxy for the W isotopic composition of the pre-late veneer terrestrial mantle (Thiemens et al., 2019), but there are no other independent constraints on this value. In this way, late accretion and core-mantle interaction may have worked together to set the $\mu^{182}W$ composition of the bulk mantle.

The timescale of putative core-mantle interactions after late accretion is not specified in the model, but may have been long-lived. For example, if core-mantle equilibration via plumes began at 4.2 Ga and continued into modern times, the 13 ppm shift in $\mu^{182}W$ compositions predicted by the model would have a rate of ~3 ppm/Ga, assuming that the modern BSE has $\mu^{182}W \approx 0$. Such changes would not currently be analytically detectible on 1-2 Ga timescales, and thus may provide an alternative explanation as to why there is no apparent secular trend in the $\mu^{182}W$

615 composition of mantle-derived rocks through the Archean. Alternatively, an Archean plume flux
616 that is more vigorous than what is observed in the modern mantle may have rapidly altered the
617 bulk mantle $\mu^{182}W$ after core-mantle interactions began. Differentiating between these two
618 scenarios is difficult given existing data. For example, recent data for crustal rocks from the North
619 China Craton have been interpreted to reflect a rapid $\mu^{182}W$ shift at 3.6 Ga corresponding to a
620 major global event, such as the onset of modern-type plate tectonics (Mei et al., 2020). On the
621 other hand, 2.9 Ga granitic rocks from the Slave Craton record positive $\mu^{182}W$ anomalies, implying
622 that mantle homogenization processes were more sluggish. Additional $\mu^{182}W$ data highlighting
623 rocks of Meso-Neoarchean age will be key to resolving this distinction.
624
625 **5. Summary and Conclusion**
626 New Nd-Hf-W isotopic data are presented for Réunion hotspot basalts that record evidence
627 for a persistent Hadean mantle domain within the Réunion plume source reservoir. Combining Nd
628 and W isotopic data provides a powerful means to interrogate Hadean processes that were critical
629 to the development of the modern Earth, such as core segregation and early crust formation.
630 Réunion and Deccan lavas preserve negative $\mu^{182}W$ compositions, some of which are resolved
631 from the terrestrial standard. Combined with the heterogeneous $\mu^{142}Nd$ composition of the lavas,
632 these data preserve a possible negative trend between the two systems. A model is constructed that
633 invokes core interaction with a trace-element enriched remnant of a Hadean magma ocean. This
634 material is then assimilated into a trace-element depleted magma ocean relic (possibly analogous
635 to BEAMS; Ballmer et al. 2017) and the combined domain subsequently incorporates a small
636 amount of recycled Hadean mafic crust. The results of this model permit interpretation of Nd-Hf
637 long-lived radiogenic isotope signatures along the mantle array (Chauvel et al., 2008) in an early

638 Earth context. These results are consistent with recent interpretations of the Sr-Nd-Pb isotopic
639 signature of Réunion lavas (Nauret et al., 2019) and recent models of the He-W isotopic signatures
640 of global OIB (Mundl-Petermeier et al., 2020). This study highlights the importance of including
641 core contributions to Earth's mantle when considering the global budget of siderophile elements
642 and other core constituents relative to contributions from late accretion. Further work is needed to
643 independently confirm the veracity of core-mantle interaction over geological timescales, as well
644 as to establish a better sense of the global Nd-W isotopic relationship and its implications for early
645 Earth processes.
646

Acknowledgements

Funding for sample collection was provided by the National Geographic Society (NGS 8330-07 to JMDD), the Geological Society of America (GSA 10539-14 to BJP), and a personal donation from Dr. R. Rex. Further support was provided by the Department of Terrestrial Magnetism, Carnegie Institution for Science, NSF (EAR-1624587 to RJW and AMP), FWF (V659-N59 to AMP), and ETH Zürich/Marie Skłodowska-Curie Actions COFUND (18-1 FEL-28 to BJP). These sources of funding are gratefully acknowledged. We thank M. Norman and four anonymous reviewers for their comments, which substantially improved the quality of the manuscript, and we thank J. Blichert-Toft for her editorial handling of this manuscript.

New datasets for this research are included in this paper and its supplementary information files, and additionally in the EarthChem database at https://doi.org/10.26022/IEDA/111786. Compiled data are referenced in the respective table and figure captions.

Table 1. Geochemical data for Réunion and Deccan igneous rocks. Samples prefixed CH and RU are from Réunion, those prefixed DC are Deccan CFB, and the sample prefixed MR is from Mauritius. "*Assim. Corr.*" refers to assimilation-corrected values (*Section 4.2*). Data in bold are new contributions from this study.

Sample	Description*	$^{3}He/^{4}He$ (R/R_A)	$\mu^{142}Nd$ [6]	2σ s.d. [6]	$\varepsilon^{143}Nd_{CHUR}(T)$ [6]	2σ s.d. [6]	n (n_d) [7]	$\varepsilon^{176}Hf_{CHUR}(T)$ [6]	2σ s.d. [6]	n (n_d) [7]	ppb W [8]	$\mu^{182}W$ [6]	2σ s.d. [6]	n (n_d) [7]
CH0702 [1,2]	Cumulate dunite, PDLF 3	13.7									**169**	**-4.3**	**4.3**	**1 (1)**
CH0704CL [3]	PDLF 3		3.7	3.3	3.89	0.07	2 (1)	**9.51**	**0.22**	**4 (1)**				
RU0702 [2,3]	PDLF 4, AD 1931	12.9	1.5	3.1	4.24	0.01	2 (1)	**8.80**	**0.19**	**6 (1)**	**167**	**-4.9**	**4.1**	**2 (2)**
RU0703 [2,3]	PDLF 4, AD 1998	12.5	-2.9	1.9	4.34	0.02	4 (1)	**9.22**	**0.19**	**6 (2)**	**315**	**-4.1**	**2.6**	**2 (2)**
RU0705 [2,3]	PDLF 4, AD 2007	13.7	4.7	2.5	4.37	0.27	2 (2)	**8.79**	**0.37**	**3 (1)**	**114**	**-4.8**	**3.1**	**1 (1)**
RU0706 [3]	PDLF 4, AD 2007		2.4	3.1	4.52	0.13	2 (1)	**9.15**	**0.27**	**4 (2)**				
RU0707 [3]	PDLF 4, AD 2001		3.8	5.3	4.32	0.01	1 (1)	**8.61**	**0.14**	**10 (2)**				
RU0708 [2,3]	PDLF 4, AD 1937	12.6	5.4	2.2	4.46	0.02	3 (1)	**8.77**	**0.18**	**6 (2)**	**253**	**-7.5**	**1.7**	**3 (2)**
RU0709 [3]	PDLF 4		6.2	2.8	4.32	0.08	3 (1)	**8.92**	**0.18**	**7 (2)**	**290**	**-6.4**	**2.4**	**1 (1)**
RU0710 [2,3]	PDN 1	12.5	-2.1	2.5	4.28	0.16	2 (2)	**8.56**	**0.22**	**4 (1)**				
RU0711 [2,3]	PDN 1	12.0	-7.9	2.9	4.05	0.05	3 (2)	**8.86**	**0.15**	**8 (2)**	**167**	**-2.9**	**3.0**	**1 (1)**
RU0712 [2,3]	PDN 1	12.8	0.0	3.1	3.85	0.01	2 (1)	**8.35**	**0.16**	**7 (2)**	**130**	**-9.6**	**4.2**	**1 (1)**
RU0714 [3]	PDN 1		5.1	2.8	4.01	0.29	2 (1)	**9.34**	**0.49**	**1 (1)**				
RU0715 [3]	PDN 3		-1.0	3.1	4.41	0.01	2 (1)	**9.01**	**0.17**	**7 (2)**				
RU0716 [3]	PDN 2		5.8	2.3	4.73	0.02	4 (1)	**9.28**	**0.15**	**8 (2)**				
RU0717 [3]	PDLF 1		-2.5	3.2	3.93	0.01	1 (1)	**8.46**	**0.19**	**5 (1)**				
RU0718 [3]	PDLF 2		5.4	3.6	4.37	0.01	1 (1)	**8.87**	**0.16**	**7 (2)**				
RU0719 [3]	PDLF 4, AD 1977		4.2	2.2	4.11	0.04	3 (1)	**8.66**	**0.20**	**5 (2)**				
RU1515 [3]	PDLF 3		2.7	3.2	3.87	0.01	7 (6)							
RU1516B [3]	PDLF 3		1.2	3.5	3.85	0.10	2 (1)	**8.17**	**0.44**	**1 (1)**				
RU1517 [3]	PDLF 3		-1.5	2.1	3.86	0.04	3 (1)	**8.33**	**0.21**	**4 (2)**				
MR0709 [2]	Older Series	10.36	**5.6**	**2.1**	**4.48**	**0.01**	**3 (1)**	**9.42**	**0.12**	**7 (2)**				
DC1405 [4]	Deccan Traps, Kutch	4.2	**6.6**	**2.5**	**0.17**	**0.01**	**2 (1)**	**-1.00**	**0.14**	**6 (2)**		**-7.0**	**3.0**	**2 (2)**
Assim. Corr.			7.6	2.8								**-14.1**	**6.0**	
DC1447B [4, 11]	Deccan Traps, Pavagadh	10.7	**11.3**	**1.5**	**1.16**	**0.03**	**7 (5)**	**5.54**	**0.14**	**7 (2)**	**163**	**-4.7**	**6.6**	**1 (1)**
Assim. Corr.			12.5	1.7								**-6.8**	**9.7**	
BHVO-2 [5, 10, 11]	USGS Reference Material		**3.7**	**3.4**	**6.66**	**0.03**	**2 (2)**	**11.27**	**0.10**	**12 (4)**	**251**	**-6.7**	**2.4**	**4 (2)**

			$\mu^{142}Nd$	Avg. RSD [9]			Avg. RSD [9]			Avg. RSD [9]		$\mu^{182}W$	Avg. RSD [9]
	Standard reference material	JNdi	0	4.5	JNdi	0.04		JMC475	0.44		Alfa Aesar	0	3.9

Notes

1: Dunite cumulate xenolith
2: He isotopic data from Furi et al (2011)
3: Nd isotopic data from Peters et al. (2018)
4: He isotopic data from Peters et al. (2017)
5: W concentration from Mundl et al. (2017)
6: Weighted averages and precision calculated using Isoplot, if n > 1. See text for details.
7: n - number of runs; n_d - numer of digestions
8: Determined by isotope dilution
9: Average 2σ s.d. of internal standards for each analytical session. See Supplementary Tables for details.
10: W isotopic data from Peters et al. (2019)
11: Some (DC1447B) or all (BHVO-2) Nd isotopic measurements performed at ETH

*Descriptions refer to the stratigraphy of McDougall (1971) for Réunion (PDN: Piton des Neiges; PDLF: Piton de la Fournaise) and Baxter (1975) for Mauritius

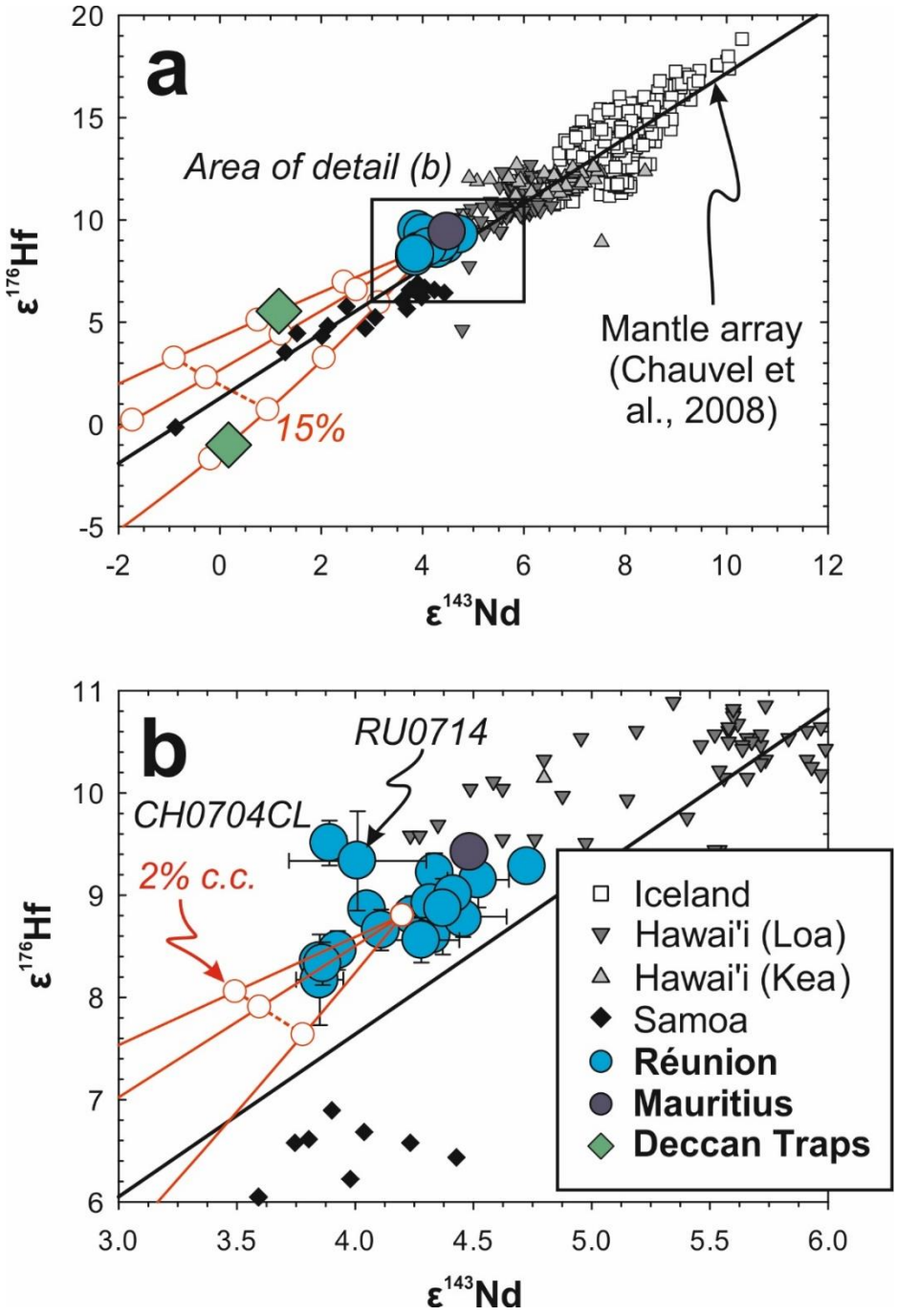

Figure 1. Neodymium-hafnium isotopic compositions of Réunion hotspot lavas with other OIB plotted for reference. Red lines model assimilation of bulk continental crust with trace element abundances from Rudnick & Gao (2003) or fitted to the Deccan samples. Circles along the model lines represent 5% increments of mixing in panel (a). Model parameters are listed in **Table S4**. Data sources: Stracke et al. (2003), Kitagawa et al. (2008), Yamasaki et al. (2009), Hanano et al. (2010), Hanyu et al. (2010), Peate et al. (2010), Chekol et al. (2011), Salters et al. (2011), Weis et al. (2011), Koorneef et al. (2012), Nobre Silva et al. (2013), Sims et al. (2013). MORB field is after Salters & Stracke (2004).

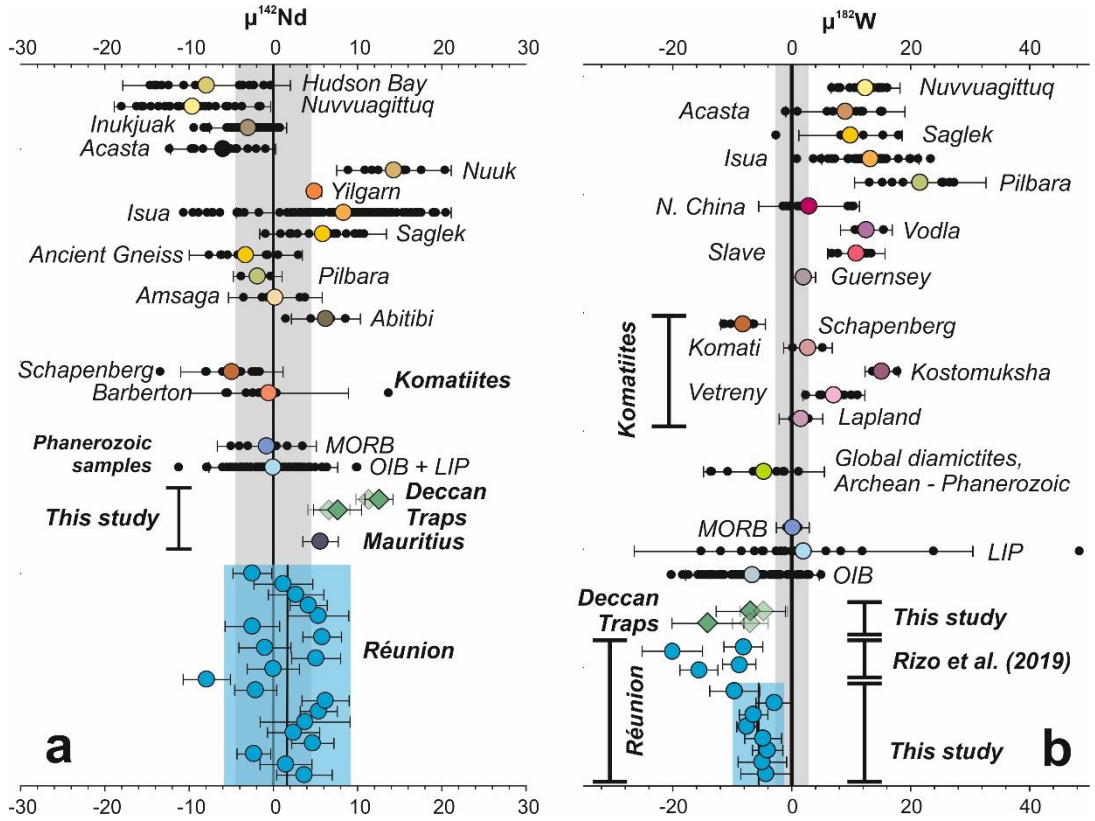

Figure 2. Short-lived radiogenic isotope composition of Réunion hotspot lavas with crustal and intraplate samples plotted for reference. Transparent symbols for Deccan CFB represent measured values uncorrected for crustal assimilation; solid symbols represent corrected values. The precision window depicted by the gray field is set to the average external precision reported in this study. Data sources, panel (a): Caro et al. (2003, 2017), Bennett et al. (2007), Andreasen et al. (2008), O'Neil et al. (2008, 2016), Murphy et al. (2010), Rizo et al., (2011, 2012, 2013, 2016a, 2016b, 2019), Cipriani et al. (2012), Jackson & Carlson (2012), Debaille et al. (2013), Puchtel et al. (2016a), Morino et al. (2017), O'Neil & Carlson (2017), Horan et al. (2018), Peters et al. (2018), Reimink et al. (2018, 2020), Saji et al. (2018), Schneider et al. (2018), Wainwright et al. (2019), Archer et al. (2019); panel (b): Willbold et al. (2011, 2015), Touboul et al. (2012, 2014), Liu et al. (2016), Puchtel et al. (2016a, 2016b, 2020), Rizo et al. (2016a, 2016b, 2019), Dale et al. (2017), Mundl et al. (2017), Kruijer & Kleine (2018), Mei et al. (2018, 2020), Mundl-Petermeier et al. (2018, 2019, 2020), Reimink et al. (2018, 2020), Archer et al. (2019), Tusch et al. (2019).

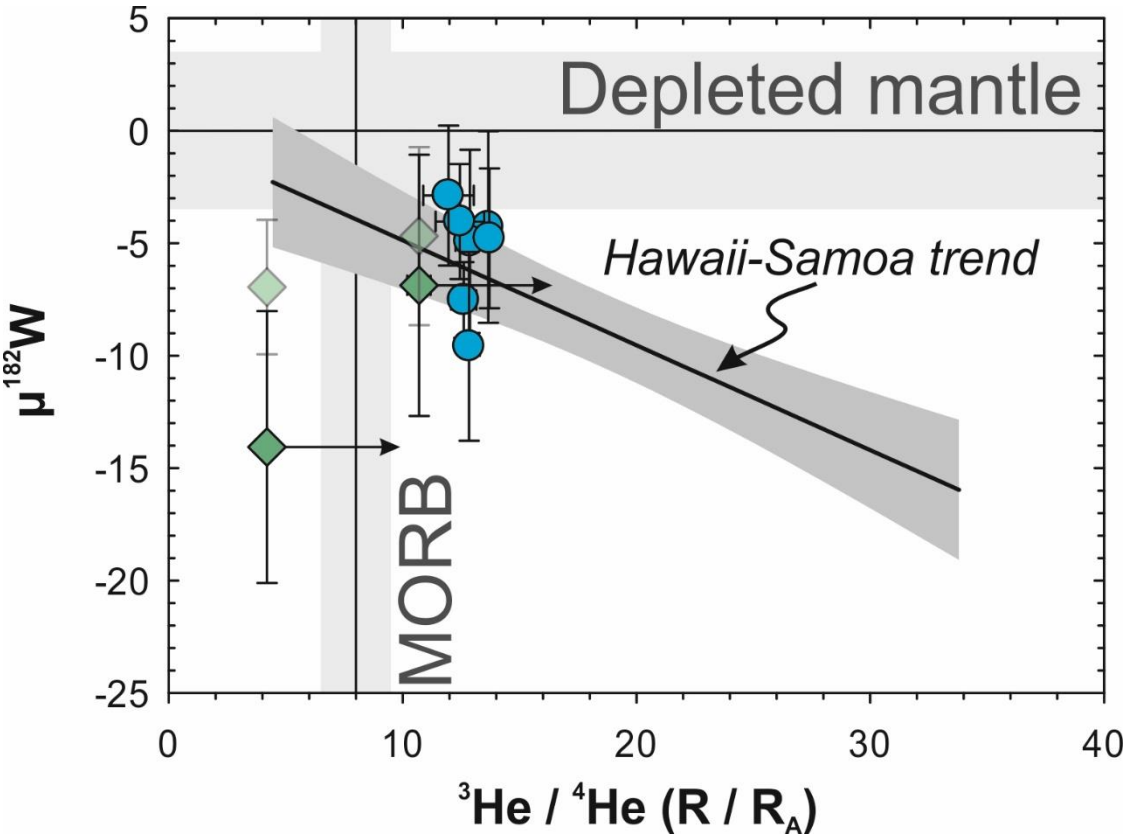

685

686 **Figure 3.** Helium and W isotopic compositions of Réunion hotspot lavas (Füri et al., 2011; Peters
687 & Day, 2017, this study) compared to the systematics of Hawai'i and Samoa OIB (Mundl et al.,
688 2017 and references therein). Symbols are as in **Figure 2**. The right-pointing arrows on the Deccan
689 samples reflect the likelihood that their $^{3}He/^{4}He$ has also been modified by crustal assimilation,
690 but to an unconstrained extent. The horizontal shaded region reflects the average precision of W
691 standard measurements during this study. The vertical shaded region reflects an approximate
692 MORB $^{3}He/^{4}He$ composition of 8 ±1.5 R_A (Graham, 2002).

693

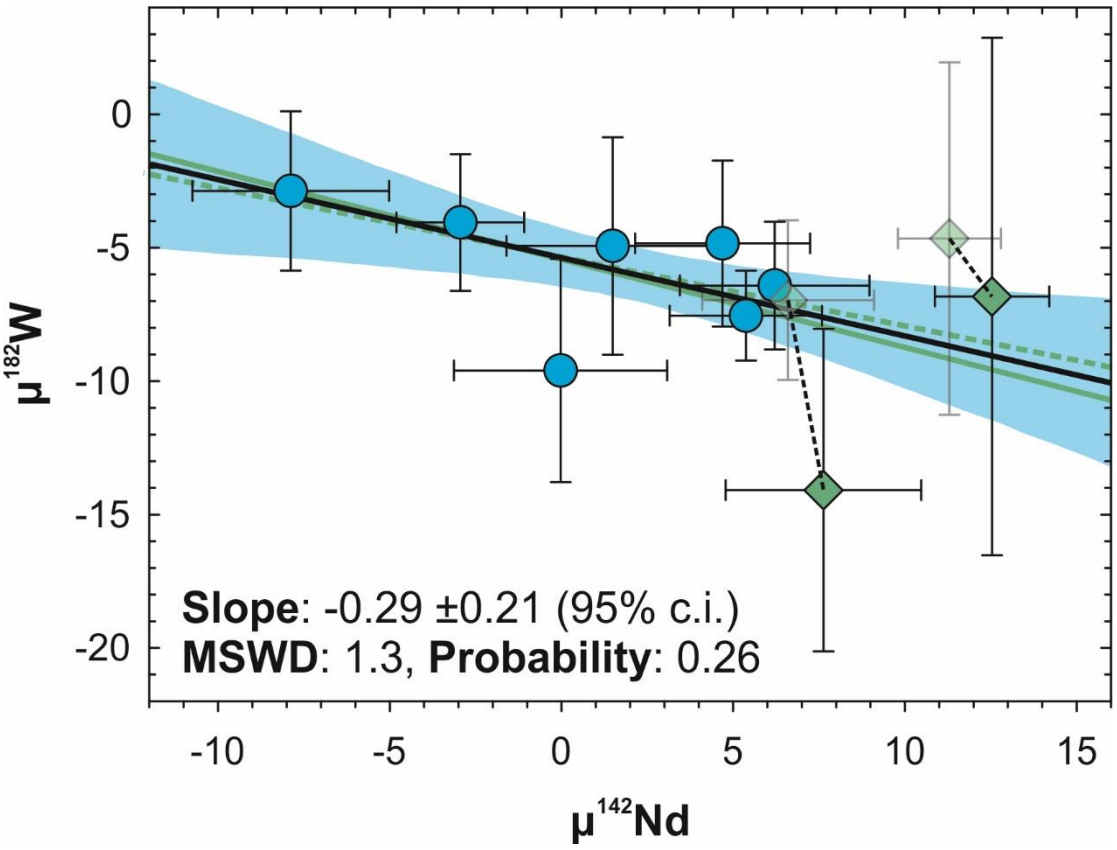

694

695 **Figure 4.** $\mu^{182}W$ versus $\mu^{142}Nd$ compositions for Réunion hotspot lavas. Black regression line and
696 blue uncertainty envelope (95% confidence interval) are calculated for Réunion OIB only (blue
697 circles). Solid green regression line is calculated for Réunion OIB plus crustal assimilation-
698 corrected Deccan CFB (solid green diamonds). Dashed green regression line is calculated for
699 Réunion OIB plus Deccan CFB that are not corrected for crustal assimilation (transparent green
700 diamonds). For a discussion of regression statistics, see *Results*.

701

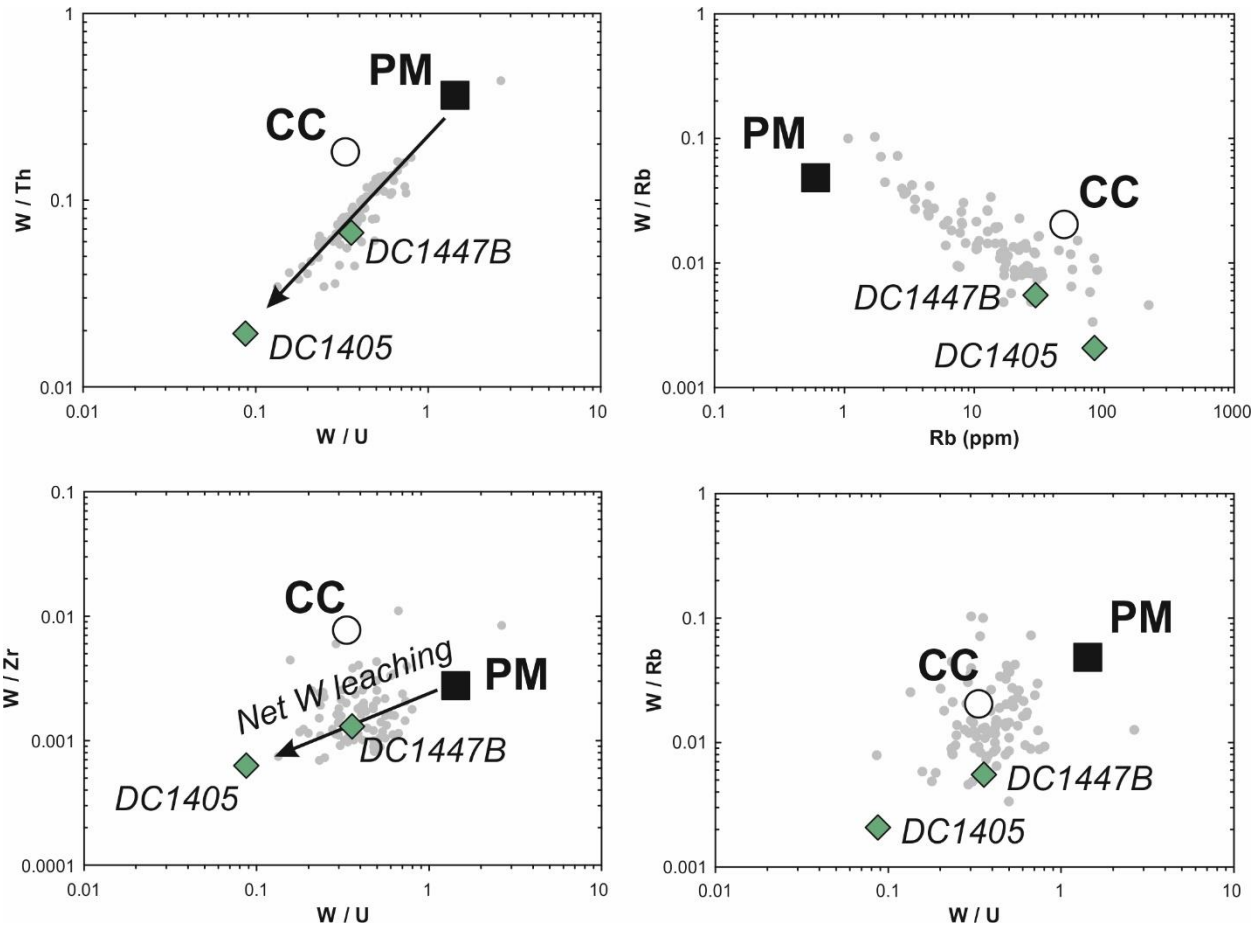

Figure 5. Plots of correlations between W/U and W/Zr, W/Th (less fluid-mobile elements), and W/Rb (more fluid-mobile) ratios. Arrows show the direction of predicted net loss of W by post-emplacement alteration (i.e., leaching of W). Small gray circles are Deccan CFB data from Peters & Day (2017), otherwise symbols are as in Figure 2. PM: primitive mantle (McDonough & Sun, 1995), CC: bulk continental crust (Rudnick & Gao, 2003).

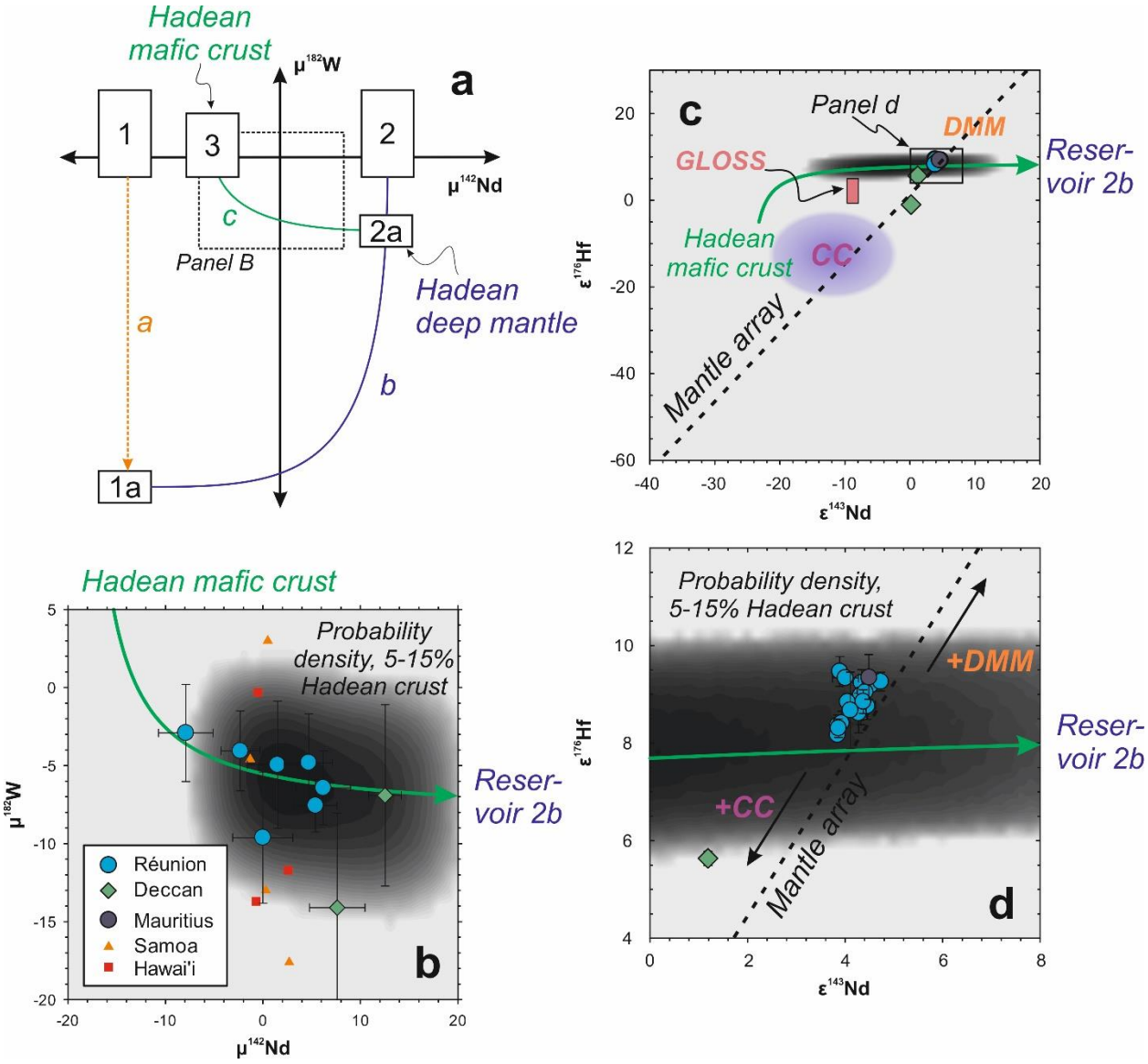

709

710 **Figure 6.** (a) Qualitative model for the $\mu^{182}W$ and $\mu^{142}Nd$ compositions of Réunion hotspot lavas.
711 (b) Probability density (darker: more probable), n = 10000 of results of a Monte Carlo simulation
712 predicting mixing trends along an example mixing line c with an example mixing line (green) for
713 reference. (c) The result of the same model for ^{143}Nd-^{176}Hf compositions, enlarged around the
714 Réunion data in (d). DMM: depleted MORB mantle; GLOSS: global subducted sediment (Plank
715 & Langmuir, 1998; Chauvel et al., 2008); CC: continental crust (Himalayan sediments from
716 Richards et al., 2005 as used in the crustal assimilation correction). See text for model details;
717 model parameters are listed in **Table S5**.

718

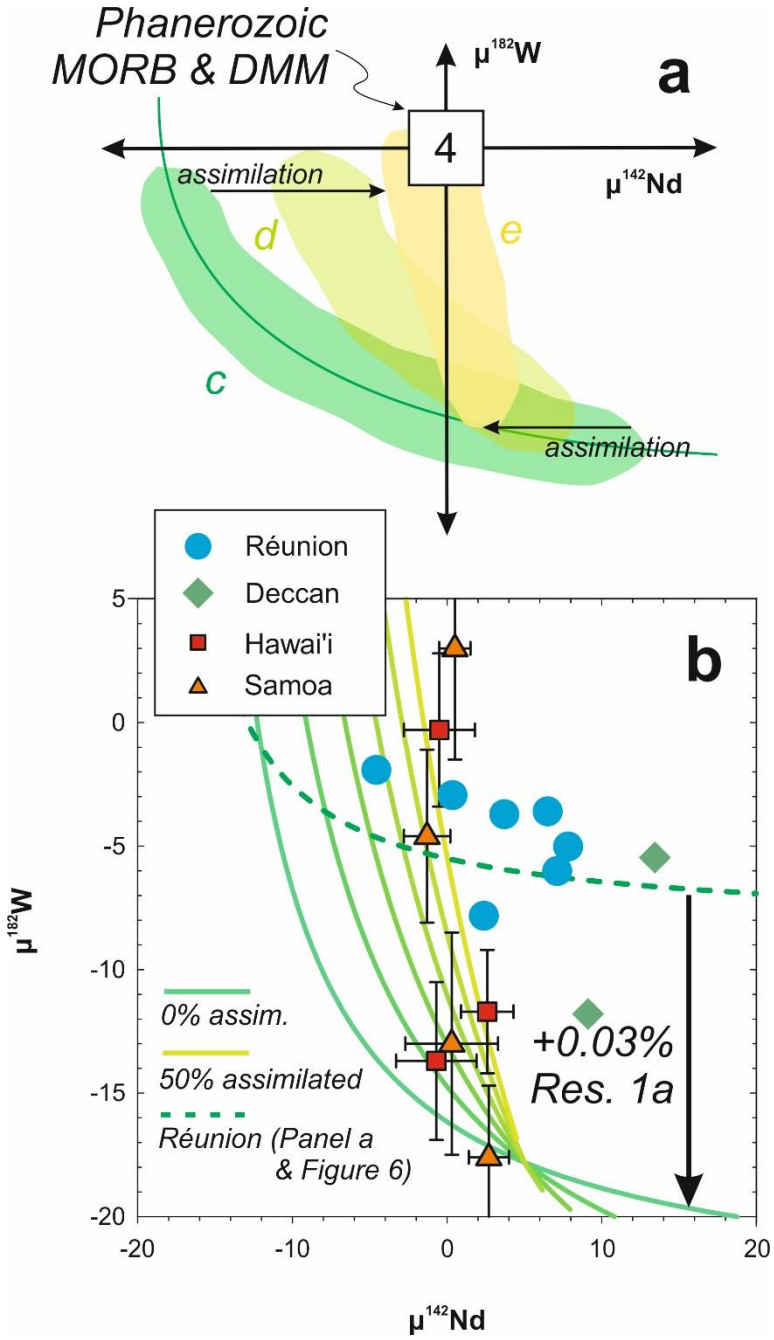

719 **Figure 7.** Qualitative (a) and quantitative (b) model of the effects of assimilating young geologic
720 material into mantle domains with Hadean Nd-W isotopic signatures. Mixing line c is identical to
721 the one in **Figure 6**. Example mixing lines simulating the effects of assimilating 0-50%
722 assimilation of post-Hadean recycled material with $\mu^{182}W = \mu^{142}Nd = 0$ and Nd/W = 3500. See
723 text for model details.

724

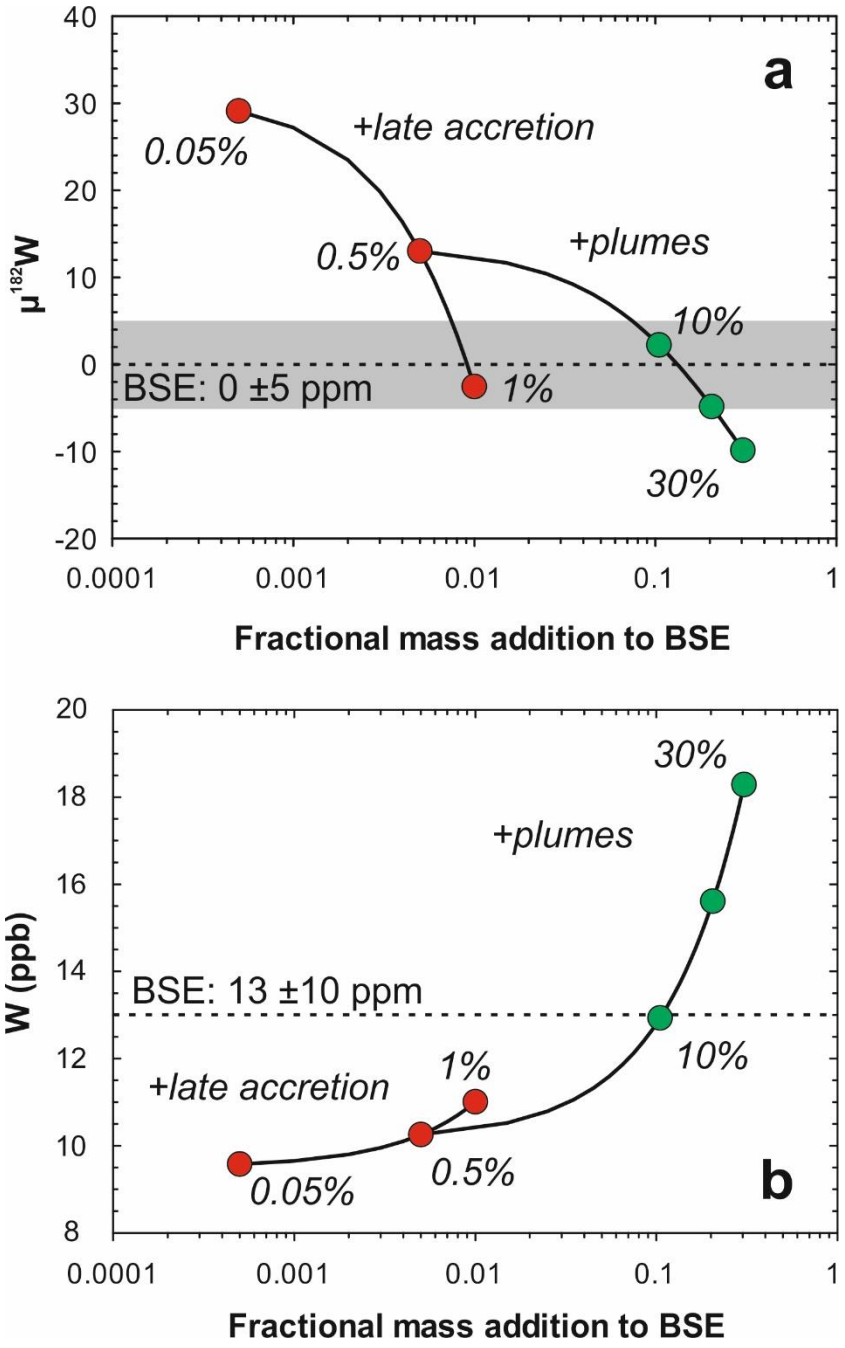

725

726 **Figure 8.** Model of the W abundance and W isotopic composition of the mantle accounting for
727 late accretion and mantle plume contributions to the silicate Earth. See *Section 4.5* for model
728 details, model parameters are listed in **Table S6**.

729

References

Adam, J. and T. Green (2006) Trace element partitioning between mica- and amphibole-bearing garnet lherzolite and hydrous basanitic melt: 1. Experimental results and the investigation of controls on partitioning behavior: Contributions to Mineralogy and Petrology, 152, 1-17.

Albarède, F., B. Luais, G. Fitton, M. Semet, E. Kaminski, B.G.J. Upton, P. Bachélery an J.-L. Cheminée (1997) The geochemical regimes of Piton de la Fournaise Volcano (Réunion) during the last 530,000 years: Journal of Petrology, 38(2), 171-201.

Andreasen, R., Sharma, M., Subbarao, K. V., & Viladkar, S. G. (2008). Where on Earth is the enriched Hadean reservoir? Earth and Planetary Science Letters, 266(1), 14-28.

Archer, G.J., Mundl, A., Walker, R.J., Worsham, E.A., and Bermingham, K.R. (2017) High-precision analysis of $^{182}W/^{184}W$ by negative thermal ionization mass spectrometry: Per-integration corrections using measured $^{18}O/^{16}O$. International Journal of Mass Spectrometry, 414, 80-86.

Archer, G.J., Brennecka, G.A., Gleissner, P., Stracke, A., Becker, H., and Kleine, T. (2019) Lack of late-accreted material as the origin of ^{182}W excesses in the Archean mantle: Evidence from the Pilbara Craton, Western Australia. Earth and Planetary Science letters, 528, doi:10.1016/j.epsl.2019.115841

Arevalo, R.A., and McDonough, W.F. (2008) Tungsten geochemistry and implications for understanding the Earth's interior. Earth and Planetary Science Letters, 272, 656-665.

Ballmer, M.D., Houser, C., Hernlund, J.W., Wentzcovitch, R.M., and Hirose, K. (2017) Persistence of strong silica-enriched domains in the Earth's lower mantle. Nature Geoscience, 10, 236-240.

Baxter, A.N. (1975) Petrology of the Older Series lavas from Mauritius, Indian Ocean. Geological Society of America Bulletin, 89, 90-101.

Bennett, V.C., Nutman, A.P., and Esat, T.M. (2002) Constraints on mantle evolution from 187Os/188Os isotopic compositions of Archean ultramafic rocks from southern West Greenland (3.8 Ga) and Western Australia (3.46 Ga). Geochimica et Cosmochimica Acta, 66(14), 2615-2630.

Bennett, V.C., Brandon, A.D., and Nutman, A.P. (2007) Coupled ^{142}Nd-^{143}Nd isotopic evidence for Hadean mantle dynamics. Nature 318, 1907-1910.

Bosch, D., Blichert-Toft, J., Moynier, F., Nelson, B.K., Telouk, P., Gillot, P.-Y. and Albarede, F. (2008) Pb, Hf and Nd isotope compostiions of the two Réunion volcanoes (Indian Ocean): A tale of two small-scale mantle "blobs"? Earth and Planetary Science Letters, 265, 748-765.

Bouhifd, M.A., Jephcoat, A.P., Porcelli, D., Kelley, S.P., and Marty, B. (2020) Potential of Earth's core as a reservoir for noble gases: Case for helium and neon. Geochemical Perspectives Letters, 15, 15-18, doi:10.7185/geochemlet.2028

Brandon, A.D., Walker, R.J., Morgan, J.W., Norman, M.D., and Prichard, H.M. (1998) Coupled ^{186}Os and ^{187}Os evidence for core-mantle interaction. Science, 280, 1570-1573.

769 Brown, S.M., Elkins-Tanton, L., and Walker, R.J. (2014) Effects of magma ocean crystallization
770 and overturn on the development of ^{142}Nd and ^{182}W isotopic heterogeneities in the
771 primordial mantle. Earth and Planetary Science Letters, 408, 319-330.

772 Carlson, R.W., Garçon, M., O'Neil, J., Reimink, J., and Rizo, H. (2019) The nature of Earth's
773 first crust. Chemical Geology, 530, 119321, doi:10.1016/j.chemgeo.2019.119321.

774 Caro, G., Bourdon, B., Birck, J.-L., and Moorbath, S. (2003) ^{146}Sm-^{142}Nd evidence from Isua
775 metamorphosed sediments for early differentiation of the Earth's mantle. Nature, 423, 428-
776 432.

777 Caro, G., B. Bourdon, B.J. Wood and A. Corgne (2005) Trace-element fractionation in Hadean
778 mantle generated by melt segregation from a magma ocean: Nature, 436, 246-249.

779 Caro, G, Bourdon, B., Birck, J.-L., and Moorbath, S. (2006) High-precision ^{142}Nd/^{144}Nd
780 measurements in terrestrial rocks: Constraints on the early differentiation of the Earth's
781 mantle. Geochimica et Cosmochimica Acta 70, 164-191, doi:10.1016/j.gca.2005.08.015

782 Caro, G., Morino, P., Mojzsis, S. J., Cates, N. L., and Bleeker, W. (2017). Sluggish Hadean
783 geodynamics: Evidence from coupled ^{146,147}Sm–^{142,143}Nd systematics in Eoarchean
784 supracrustal rocks of the Inukjuak domain (Québec). Earth and Planetary Science
785 Letters, 457, 23-37.

786 Chauvel, C., Lewin, E., Carpentier, M., Arndt, N.T., and Marini, J.-C. (2008) Role of recycled
787 oceanic basalt and sediment in generating the Hf-Nd mantle array. Nature Geoscience 1,
788 64-67.

789 Chekol, T.A., Kobayashi, K., Yokoyama, T., Sakaguchi, and Nakamura, E. (2011) Timescales of
790 magma differentiation from basalt to andesite beneath Hekla Volcano, Iceland: Constraints
791 from U-series disequilibria in lavas from the last quarter-millenium flows. Geochemica et
792 Cosmochimica Acta, 75, 256-283.

793 Chou, C.-L. (1978) Fractionation of siderophile elements in the earth's upper mantle.
794 Proceedings of the Lunar and Planetary Science Conference, 9, 219-230.

795 Cipriani, A., Bonatti, E., and Carlson, R. W. (2011). Nonchondritic ^{142}Nd in suboceanic mantle
796 peridotites. Geochemistry, Geophysics, Geosystems, 12(3).

797 Corgne, A., C. Liebske, B.J. Wood, D.C. Rubie, and D.J. Frost (2005) Silicate perovskite-melt
798 partitioning of trace elements and geochemical signature of a deep perovskitic reservoir.
799 Geochimica et Cosmochimica Acta, 69(2), 485-496.

800 Dauphas, N. (2017) The isotopic nature of the Earth's accreting material through time. Nature,
801 541, 521-524.

802 Davies, G.F. (1992) Temporal variation of the Hawaiian plume flux. Earth and Planetary Science
803 Letters, 113, 277-286.

804 Dale, C.W., Kruijer, T.S., and Burton, K.W. (2017) Highly siderophile element and 182W
805 evidence for a partial late veneer in the source of 3.8 Ga rocks from Isua, Greenland. Earth
806 and Planetary Science Letters, 458, 394-404, doi:10.1016/j.epsl.2016.11.001

807 Day, J.M.D. (2013) Hotspot volcanism and highly siderophile elements. Chemical Geology, 341,
808 50-74, doi:10.1016/j.chemgeo.2012.12.010.

Debaille, V., O'Neill, C., Brandon, A. D., Haenecour, P., Yin, Q. Z., Mattielli, N., and Treiman, A. H. (2013). Stagnant-lid tectonics in early Earth revealed by ^{142}Nd variations in late Archean rocks. Earth and Planetary Science Letters, 373, 83-92.

Devey, C.W., and Lightfoot, P.C. (1986) Volcanological and tectonic control of stratigraphy and structure in the western Deccan Traps. Bulletin of Volcanology, 48, 195-207.

Friedman, A.M., J. Milsted, D. Metta, D. Henderson, J. Lerner, A.L. Harkness and D.J. Rok Op (1966) Alpha decay half lives of ^{148}Gd ^{150}Gd and ^{146}Sm: Radiochimica Acta, 5(4).

Füri, E., D.R. Hilton, B.J. Murton, C. Hémond, J. Dyment and J.M.D. Day (2011) Helium isotope variations between Réunion Island and the Central Indian Ridge (17°-21°S): new evidence for ridge-hot spot interaction: Journal of Geophysical Research, 116, B02207.

Garçon, M., Boyet, M., Carlson, R.W., Horan, M.F., Auclair, D., and Mock, T.D. (2018) Factors influencing the precision and accuracy of Nd isotope measurements by thermal ionization mass spectrometry. Chemical Geology 476, 493-514.

Gautam, I., Ray, J.S., Bhutani, R., Balakrishnan, S., and Dash, J.K. (2017) Role of fractionation correction in accurate determination of ^{142}Nd/^{144}Nd by TIMS: A case study of 1.48 Ga alkaline rocks from Khariar, India. Chemical Geology, 466, 479-490, doi:10.1016/j.chemgeo.2017.06.036

Gillot, P.-Y., Lefèvre, J.-C. and Nativel, P.-E. (1994) Model for the structural evolution of the volcanoes of Réunion Island. Earth and Planetary Science Letters 122, 291-302.

Graham, D.W. (2002) Noble gas isotope geochemistry of mid-ocean ridge and ocean island basalts: Characterization of mantle source reservoirs. *In* Porcelli, D., Ballentine, C.J., and Wieler, R. (eds.) Noble gases in geochemistry and cosmochemistry. Reviews in Mineralogy and Geochemistry, 47, 247-317.

Guitreau, M., Mukasa, S.B., Loudin, L., and Krishnan, S. (2017) New constraints on the early formation of the Western Dharwar Craton (India) from igneous zircon U-Pb and Lu-Hf isotopes. Precambrian Research 302, 33-49, doi: 10.1016/j.precamres.2017.09.016

Hanano, D., Weis, D., Schoates, J.S., Aciego, S., and DePaolo, D.J. (2010) Horizontal and vertical zoning of heterogeneities in the Hawaiian mantle plume from the geochemistry of consecutive postshield volcano pairs: Kohala-Mahukona and Mauna Kea-Hualalai. Geochemistry Geophysics Geosystems, 11(1), doi:10.1029/2009GC002782.

Hanyu, T., Kimura, J.-I., Katakuse, M., Calvert, A.T., Sisson, T.W. and Nakai, S. (2010) Source materials for inception stage Hawaiian magmas: Pb-He isotope variations for early Kilauea. Geochemistry, Geophysics, Geosystems 11, doi:10.1029/2009GC002760.

Hofmann, C., Feraud, G., and Courtillot, V. (2000) ^{40}Ar/^{39}Ar dating of mineral separates and whole rocks from the Western Ghats lava pile: further constraints on the duration and age of the Deccan Traps. Earth and Planetary Science Letters 180, 13-27.

Holzapfel, C., Rubie, D.C., Frost, D.J., and Langenhorst, F. (2005) Fe-Mg interdiffusion in (Mg,Fe)SiO_3 perovskite and lower mantle reequilibration. Science, 309, 1707.

Horan, M., Carlson, R.W., Walker, R.J., Jackson, M., and Mundl, A. (2018) Tracking Hadean processes in modern basalts. Earth and Planetary Science Letters 484, 184-191.

Humayun, M. (2011) A model for osmium isotopic evolution of metallic solids at the core-mantle boundary: Geochemistry Geophysics Geosystems, 12(3), 23 pp.

Jackson, M.G. and Carlson, R.W. (2012) Homogeneous superchondritic $^{142}Nd/^{144}Nd$ in the mid-ocean ridge basalt and ocean island basalt mantle. Geochemistry Geophysics Geosystems 13, doi:10.1029/2012GC004114.

Jackson, M.G., Shirey, S.B., Hauri, E.H., Kurz, M.D. and Rizo, H. (2016) Peridotite xenoliths from the Polynesian Austral and Samoa hotspots: Implications for the destruction of ancient ^{187}Os and ^{142}Nd isotopic domains and the preservation of Hadean ^{129}Xe in the modern convecting mantle. Geochimica et Cosmochimica Acta 185, 21-43.

Jackson, M.G., Blichert-Toft, J., Halldórsson, S.A., Mundl-Petermeier, A., Bizimis, M., Kurz, M.D., Price, A.A., Harðardóttir, S., Willhite, L.N., Breddam, K., Becker, T.W., and Fischer, R.A. (2020) Ancient helium and tungsten isotopic signatures preserved in mantle domains least modified by crustal recycling. Proceedings of the National Academy of Sciences, 117(49), 30993-31001, doi:10.1073/pnas.2009663117.

Kitagawa, H., Kobayashi, K., Makishima, A., and Nakamura, E. (2008). Multiple pulses of the mantle plume: evidence from Tertiary Icelandic lavas. Journal of Petrology, 49(7), 1365-1396.

Kleine, T., Mezger, K., Münker, C., Palme, H., and Bischoff, A. (2004) 182Hf-182W isotope systematics of chondrites, eucrites, and martial meteorites: Chronology of core formation and early mantle differentiation in Vesta and Mars. Geochimica et Cosmochimica Acta, 68(13), 2935-2946, doi:10.1016/j.gca.2004.01.009

Koorneef, J.M., Stracke, A., Bourdon, A., Meier, M.A., Jochum, K.P., Stoll, B., and Grönvold, K. (2012) Melting of a two-component source beneath Iceland. Journal of Petrology, 53(1), 127-157, doi:10.1093/petrology/egr059.

König, S., Münker, C., Schuth, S., and Garbe-Schönberg, D. (2008). Mobility of tungsten in subduction zones. Earth and Planetary Science Letters, 274(1), 82-92.

Kruijer, T.S., and Kleine, T. (2018) No ^{182}W excess in the Ontong Java Plateau source. Chemical Geology, 485, 24-31, doi:10.1016/j.chemgeo.2018.03.024

Kruijer, T.S., Kleine, T., Fischer-Gödde, M., and Sprung, P. (2015) Lunar tungsten isotopic evidence for the late veneer. Nature, 520, 537-540, doi:10.1038/nature14360

Labrosse, S., Hernlund, J.W., and Coltice, N. (2007) A crystallizing dense magma ocean at the base of the Earth's mantle. Nature, 450, 866-869, doi:10.1038/nature06355

de Leeuw, G.A.M., R.M. Ellam, F.M. Stuart and R.W. Carlson (2017) $^{142}Nd/^{144}Nd$ inferences on the nature and origin of the source of high $^{3}He/^{4}He$ magmas: Earth and Planetary Science Letters, 472, 62-68.

Liu, J., Touboul, M., Ishikawa, A., Walker, R.J., and Pearson, D.G. (2016) Widespread tungsten isotope anomalies and W mobility in crustal and mantle rocks of the Eoarchean Saglek Block, northern Labrador, Canada: Implications for early Earth processes and W recycling. Earth and Planetary Science Letters 448, 13-23.

Luais, B. (2004) Temporal changes in Nd isotopic composition of Piton de la Fournaise magmatism (Réunion Island, Indian Ocean): Geochemistry, Geophysics, Geosystems, 5(1), 17 pp.

Ludwig, K.R. (2003) ISOPLOT 3.00. A geochemical toolkit for Microsoft Excel. Berkeley Geocrhonological Center Spec. Publ. No. 4, 70 pp.

Mann, U., D.J. Frost, D.C. Rubie, H. Becker and A. Audétat (2012) Partitioning of Ru, Rh, Pd, Re, Ir and Pt between liquid metal and silicate at high pressures and high temperatures – implications for the origin of highly siderophile element concentrations in Earth's mantle: Geochimica et Cosmochimica Acta, 84, 593-613.

Marchi, S., Canup, R.M., and Walker, R.J. (2018) Heterogeneous delivery of silicate and metal to the Earth by large planetesimals. Nature Geoscience, 11, 77-81.

McDonough, W.F. (1990) Constraints on the composition of the continental lithospheric mantle. Earth and Planetary Science Letters, 101, 1-18.

McDonough, W.F. and Sun, S.-s. (1995) The composition of the Earth. Chemical Geology 120, 223-253.

McDougall, I. (1971) The geochronology and evolution of the young volcanic island of Réunion, Indian Ocean. Geochimica et Cosmochimica Acta, 35, 261-288.

McNamara, A.K., E.J. Garnero and S. Rost (2010) Tracking deep mantle reservoirs with ultra low velocity zones: Earth and Planetary Science Letters, 299, 1-9 (2010).

Mei, Q.-F., Yang, J.-H., and Yang, Y.-H. (2018) An improved extraction chromatographic purification of tungsten from a silicate matrix for high precision isotopic measurements using MC-ICPMS. Journal of Analytical Atomic Spectrometry, 33, 569-577, doi:10.1039-c8ja00024g

Mei, Q.-F., Yang, J.-H., Wang, Y.-F., Wang, H., and Peng, P. (2020) Tungsten isotopic constraints on homogenization of the Archean silicate Earth: Implications for the transition of tectonic regimes. Geochimica et Cosmochimica Acta, 278, 51-64.

Melluso, L., Mahoney, J.J., and Dallai, L. (2006) Mantle sources and crustal input as recorded in high-Mg Deccan Traps basalts of Gujarat (India). Lithos, 89, 259-274.

Moore, J., White, W.M., Paul, D., Duncan, R.A., Abouchami, W. and Galer, S.J.G. (2011) Evolution of shiled-building and rejuvenescent volcanism of Mauritius: Journal of Volcanology and Geothermal Research, 207, 47-66.

Morgan, J.W., Walker, R.J., Brandon, A.D., and Horan, M.F. (2001) Siderophile elements in Earth's upper mantle and lunar breccias: Data synthesis suggest manifestation of the same late influx. Meteoritics & Planetary Science, 36, 1257-1275.

Morino, P., Caro, G., Reisberg, L., and Schumacher, A. (2017). Chemical stratification in the post-magma ocean Earth inferred from coupled $^{146,147}Sm$–$^{142,143}Nd$ systematics in ultramafic rocks of the Saglek block (3.25–3.9 Ga; northern Labrador, Canada). Earth and Planetary Science Letters, 463, 136-150.

Moyen, J.-F., and van Hunen, J. (2012) Short-term episodicity of Archaean plate tectonics. Geology, 40(5), 451-454, doi:10.1130/G322894.1

928 Mundl, A., M. Touboul, M.G. Jackson, J.M.D. Day, M.D. Kurz, V. Lekic, R.T. Helz and R.J.
929 Walker (2017) Tungsten-182 heterogeneity in modern ocean island basalts: Science, 356,
930 66-69.

931 Mundl, A., Walker, R.J., Reimink, J.R., Rudnick, R.L., and Gaschnig, R.M. (2018) Tungsten-
932 182 in the upper continental crust: Evidence from glacial diamictites. Chemical Geology
933 494, 144-152.

934 Mundl-Petermeier, A., Walker, R.J., Jackson, M.G., Blichert-Toft, J., Kurz, M.D., and
935 Haldórsson, S.A. (2019) Temporal evolution of primordial tungsten-182 and $^{3}He/^{4}He$
936 signatures in the Iceland mantle plume. Chemical Geology.

937 Mundl-Petermeier, A., Walker, R.J., Fischer, R.A., Lekic, V., Jackson, M.G., and Kurz, M.D.
938 (2020) Anomalous $\mu^{182}W$ signatures in high $^{3}He/^{4}He$ ocean island basalts – fingerprints of
939 Earth's core? Geochimica et Cosmochimica Acta, 271, 194-211
940 doi:10.1016/j.gca.2019.12.020

941 Murphy, D.T., A.D. Brandon, V. Debaille, R. Burgess and C. Ballentine (2010) In search of a
942 hidden long-term isolated sub-chondritic $^{142}Nd/^{144}Nd$ reservoir in the deep mantle:
943 Implications for the Nd isotope systematics of the Earth. Geochimica et Cosmochimica
944 Acta, 74(2), 738-750.

945 Münker, C., Weyer, S., Scherer, E., and Mezger, K. (2001) Separation of high field strength
946 elements (Nb, Ta, Zr, Hf) and Lu from rock samples for MC-ICPMS measurements.
947 Geochemistry Geophysics Geosystems 2, doi:10.1029/2001GC000183

948 Nauret, F., Famin, V., Vlastélic, I., and Gannoun, A. (2019) A trace of recycled continental crust
949 in the Réunion hotspot. Chemical Geology, 524, 67-76.

950 Nobre Silva, I.G., Weis, D., and Scoates, J.S. (2013) Isotopic systematics of the early Mauna
951 Kea shield phase and insight into the deep mantle beneath the Pacific Ocean. Geochemistry
952 Geophysics Geosystems, 14(3), doi:10.1002/ggge.20047

953 O'Neil, J., and Carlson, R. W. (2017). Building Archean cratons from Hadean mafic
954 crust. Science, 355(6330), 1199-1202.

955 O'Neil, J., Carlson, R. W., Francis, D., and Stevenson, R. K. (2008). Neodymium-142 evidence
956 for Hadean mafic crust. Science, 321(5897), 1828-1831.

957 O'Neil, J., Carlson, R.W., Paquette, J.-L., and Francis, D. (2012) Formation age and
958 metamorphic history of the Nuvvuagittuq Greenstone Belt. Precambrian Research, 220-
959 221, 23-44.

960 O'Neil, J., H. Rizo, M. Boyet, R.W. Carlson and M.T. Rosing (2016) Geochemistry and Nd
961 isotopic characteristics of Earth's Hadean mantle and primitive crust: Earth and Planetary
962 Science Letters, 442, 194-205.

963 Peate, D.W., Breddam, K., Baker, J.A., Kurz, M.D., Barker, A.K., Prestvik, T., Grassineau, N.,
964 and Skovgaard, A.C. (2010) Compositional characteristics and spatial distribution of
965 enriched Icelandic mantle components. Journal of Petrology, 51(7), 1447-1475.

966 Peng, Z.X., Mahoney, J., Hooper, P., Harris, C., and Beane, J. (1994) A role for lower crust in
967 flood basalt genesis? Isotopic and incompatible element study of the lower six formations
968 of the western Deccan Traps. Geochimica et Comsochimica Acta, 58, 267-288.

969 Peters, B.J., and Day, J.M.D. (2017) A geochemical link between plume head and tail volcanism:
970 Geochemical Perspectives Letters, 5, 29-34.

971 Peters, B.J., Day, J.M.D., Greenwood, R.C., Hilton, D.R., Gibson, J., and Franchi, I.A. (2017)
972 Helium-oxygen-osmium isotopic and elemental constraints on the mantle sources of the
973 Deccan Traps. Earth and Planetary Science Letters, 478, 245-257.

974 Peters, B.J., Carlson, R.W., Day, J.M.D., and Horan, M.F. (2018) Hadean silicate differentiation
975 preserved by anomalous $^{142}Nd/^{144}Nd$ in the Réunion hotspot source. Nature, 555, 89-93,
976 doi:1.1038/nature25754.

977 Peters, B.J., Mundl-Petermeier, A., Horan, M.F., Carlson, R.W., and Walker, R.J. (2019)
978 Chemical separation of tungsten and other trace elements for TIMS isotope ratio
979 measurements using organic acids. Geostandards and Geoanalytical Research,
980 doi:10.1111/ggr.12259.

981 Plank, T., and Langmuir, C.H. (1998) The chemical composition of subducting sediment and its
982 consequences for the crust and mantle. Chemical Geology, 145, 325-394.

983 Porcelli, D., and Halliday, A.N. (2001) The core as a possible source of mantle helium. Earth and
984 Planetary Science Letters, 192, 45-56.

985 Puchtel, I. S., Blichert-Toft, J., Touboul, M., Horan, M. F., and Walker, R. J. (2016a). The
986 coupled ^{182}W-^{142}Nd record of early terrestrial mantle differentiation. Geochemistry
987 Geophysics Geosystems, 17(6), 2168-2193.

988 Puchtel, I.S., Touboul, M., Blichert-Toft, J., Walker, R.J., Brandon, A.D., Nicklas, R.W.,
989 Kulikov, V.S., and Samsonov, A.V. (2016b) Lithophile and siderophile element
990 systematics of Earth's mantle at the Archean-Proterozoic boundary: Evidence from 2.4 Ga
991 komatiites. Geochimica et Cosmochimica Acta, 180, 227-255.

992 Puchtel, I.S., Mundl-Petermeier, A., Horan, M., Hanski, E.J., Blichert-Toft, J., and Walker, R.J.
993 (2020) Ultra-depleted 2.05 Ga komatiites of Finnish Lapland: Products of grainy late
994 accretion or core-mantle interaction? Chemical Geology, 554,
995 doi:10.1016/j.chemgo.2020.119801

996 Reimink, J.R., Chacko, T., Stern, R.A., and Heaman, L.M. (2014) Earth's earliest evolved crust
997 generated in an Iceland-like setting. Nature Geoscience, 7, 529-533,
998 doi:10.1038/NGEO02170.

999 Reimink, J.R., Chacko, T., Carlson, R.W., Shirey, S.B., Liu, J., Stern, R.A., Bauer, A.M.,
1000 Pearson, D.G., and Heaman, L.M. (2018) Petrogenesis and tectonics of the Acasta Gneiss
1001 Complex derived from integrated petrology and ^{142}Nd and ^{182}W extinct nuclide-
1002 geochemistry. Earth and Planetary Science Letters 494, 12-22,
1003 doi:10.1016/j.epsl.2016.04.047

1004 Reimink, J.R., Mundl-Petermeier, A., Carlson, R.W., Shirey, S.B., Walker, R.J., and Pearson,
1005 D.G. (2020) Tungsten isotope composition of Archean crustal reservoirs and implications
1006 for terrestrial μ182W evolution. Geochemistry, Geophysics, Geosystems, 21,
1007 doi:10.1029/2020GC009155

1008 Richards, M.A., Duncan, R.A., and Courtillot, V.E. (1989) Flood basalts and hot-spot tracks:
1009 Plume heads and tails. Science, 246, 103-107.

Richards, A., Argles, T., Harris, N., Parrish, R., Ahmad, T., Darbyshire, F., and Dragantis, E. (2005) Himalayan architecture constrained by isotopic tracers from clastic sediments. Earth and Planetary Science Letters, 236, 773-796.

Righter, K. and C.K. Shearer (2003) Magmatic fractionation of Hf and W: Constraints on the timing of core formation and differentiation in the Moon and Mars. Geochimica et Cosmochimica Acta, 67(13), 2497-2507.

Rizo, H., M. Boyet, J. Blichert-Toft and M. Rosing (2011) Combined Nd and Hf isotope evidence for deep-seated source of Isua lavas: Earth and Planetary Science Letters, 312, 267-279.

Rizo, H., Boyet, M., Blichert-Toft, J., O'Neil, J., Rosing, M. T., and Paquette, J. L. (2012). The elusive Hadean enriched reservoir revealed by ^{142}Nd deficits in Isua Archaean rocks. Nature, 491(7422), 96.

Rizo, H., Boyet, M., Blichert-Toft, J., and Rosing, M. T. (2013). Early mantle dynamics inferred from ^{142}Nd variations in Archean rocks from southwest Greenland. Earth and Planetary Science Letters, 377, 324-335.

Rizo, H., Walker, R.J., Carlson, R.W., Touboul, M., Horan, M.F., Puchtel, I.S., Boyet, M., Rosing, M.T. (2016a) Early Earth differentiation investigated through ^{142}Nd, ^{182}W, and highly siderophile element abundances in samples from Isua, Greenland. Geochimica et Cosmochimica Acta, 175, 319-336, doi:10.1016/j.gca.2015.12.007

Rizo, H., R.J. Walker, R.W. Carlson, M.F. Horan, S. Mukhopadhyay, V. Manthos, D. Francis and M.G. Jackson (2016b) Preservation of Earth-forming events in the tungsten isotopic composition of modern flood basalts: Science, 352, 809-812.

Rizo, H., Andrault, D., Bennett, N.R., Humayun, M., Brandon, A., Vlastelic, I., Moine, B., Poirier, A., Bouhifd, M.A., and Murphy, D.T. (2019) ^{182}W evidence for core-mantle interaction in the source of mantle plumes. Geochemical Perspectives Letters, 11, 6-11, doi:10.7185/geochemlet.1917

Rosas, J.C., and Korenaga, J. (2018) Rapid crustal growth and efficient crustal recycling in the early Earth: Implications for Hadean and Archean geodynamics. Earth and Planetary Science Letters, 494, 42-49.

Roth, A.S.G., Scherer, E.E., Maden, C., Mezger, K., and Bourdon, B. (2014) Revisiting the ^{142}Nd deficits in the 1.48 Ga Khariar alkaline rocks, India. Chemical Geology, 386, 238-248.

Roth, A.S.G., Liebske, C., Maden, C., Burton, K.W., Schönbächler, M., and Busemann, H. (2019) The primoridal He budget of the Earth set by percolative core formation in planetesimals. Geochemical Perspectives Letters, 9, 26-31, doi:10.7185/geochemlett.1901

Saji, N.S., Larsen, K., Wielandt, D., Schiller, M., Costa, M.M., Whitehouse, M.J., Rosing, M.T., and Bizzarro, M. (2018) Hadean geodynamics inferred from time-varying ^{142}Nd/^{144}Nd in the early Earth rock record. Geochemical Perspectives Letters, 7, 43-48, doi:10.7185/geochemlet.1818

Salters, V.J.M., and Stracke, A. (2004) Composition of the depleted mantle. Geochemistry, Geophysics, Geosystems, 5(5), Q05B07, doi:10.1029/2003GC000597.

Salters, V.J.M., Mallick, S., Hart, S.R., Langmuir, C.E., and Stracke, A. (2011) Domains of depleted mantle: New evidence from hafnium and neodymium isotopes. Geochemistry Geophysics Geosystems, 12(8), doi:10.1029/2011GC003617

Scherstén, A., Elliott, T., Hawkesworth, C., and Norman, M. (2004) Tungsten isotope evidence that mantle plumes contain no contribution from the Earth's core. Nature, 427, 234-237.

Schiano, P., David, K., Vlastélic, I., Gannoun, A., Klein, M., Nauret F. and Bonnand, P. (2012) Osmium isotope systematics of historical lavas from Piton de la Fournaise (Réunion Island, Indian Ocean). Contributions to Mineralogy and Petrology, 164(5), 805-820.

Schoene, B., Samperton, K.M., Eddy, M.P., Keller, G., Adatte, T., Bowring, S.A., Khadri, S.F.R., and Gertsch, B. (2015) U-Pb geochronology of the Deccan Traps and relation to the end-Cretaceous mass extinction. Science, 347, 182-184.

Schneider, K.P., Hoffmann, J.E., Boyet, M., Münker, C., and Kröner, A. (2018) Coexistance of enriched and modern-like ^{142}Nd signatures in Archean igneous rocks of the eastern Kappvaal Craton, southern Africa. Earth and Planetary Science Letters, 487, 54-66.

Sheth, H.C., Zellmer, G.F., Kshirsager, P.V., and Cucciniello, C. (2013) Geochemistry of the Palitana flood basalt sequence and the Eastern Saurashtra dykes, Deccan Traps: clues to petrogenesis, dyke-flow relationships, and regional lava stratigraphy. Bulletin of Volcanology, 75:701.

Sims, K.W.W., Maclennan, J., Blichert-Toft, J., Mervine, E.M., Blusztajn, J., and Grönvold, K. (2013) Short length scale mantle heterogeneity beneath Iceland probed by glacial modulation of melting. Earth and Planetary Science Letters, 379, 146-157, doi:10.1016/j.epsl.2013.07.027

Stracke, A., Zindler, A., Salters, V.J.M., McKenzie, D., Blichert-Toft, J., Albarède, F., and Grönvold, K. (2003) Theistareykir revisited. Geochemistry Geophysics Geosystems, 4(2), doi:10.1029/2001GC000201.

Talukdar, D., Pandey, A., Rao, N.V.C, Kumar, A., Pandit, D., Belyatsky, B., and Lehmann, B. (2018) Petrology and geochemistry of the Mesoproterozoic Vattikod lamproites, Eastern Dharwar Craton, southern India: evidence for multiple enrichment of sub-continental lithospheric mantle and links with amalgamation and break-up of the Columbia supercontinent. Contributions to Mineralogy and Petrology, 173(67), doi:10.1007/s00410-018-1493-y.

Thiemens, M.M., Sprung, P., Fonesca, R.O.C., Leitzke, F.P., and Münker, C. (2019) Early moon formation inferred from hafnium-tungsten systematics. Nature Geoscience, 12, 696-700, doi:10.1038/s41561-019-0398-3

Touboul, M., I.S. Puchtel and R.J. Walker (2012) ^{182}W evidence for long-term preservation of early mantle differentiation products: Science, 355, 1065-1070.

Touboul, M., J. Liu, J. O'Neil, I.S. Puchtel and R.J. Walker (2014) New insights into the Hadean mantle revealed by ^{182}W and highly siderophile element abundances of supracrustal rocks from the Nuvvuagittuq greenstone belt, Quebec, Canada: Chemical Geology, 383, 63-75.

Touboul, M., Puchtel, I.S., and Walker, R.J. (2015) Tungsten isotopic evidence for disproportional late accretion to the Earth and Moon. Nature, 520, 530-533, doi:10.1038/nature14355.

Tusch, J., Sprung, P., van de Löcht, J., Hoffmann, J.E., Boyd, A.J., Rosing, M.T., and Münker, C. (2019) Uniform 182W isotope compositions in Eoarchean rocks from the Isua region, SW Greenland: The role of early silicate differentiation and missing late veneer. Geochimica et Cosmochimica Acta, 257, 284-310, doi:10.1016/j.gca.2019.05.012

Vockenhuber, C., Oberli, F., Bichler, M., Ahmad, I., Quitté, G., Meier, M., Halliday, A.N., Lee, D.-C., Kutschera, P., Steier, P., Gehrke, R.J., and Helmer, R.G. (2004). New Half-Life Measurement of H f 182: Improved Chronometer for the Early Solar System. Physical Review Letters, 93(17), 172501.

Wainwright, A., El Atrassi, F., Debaille, V., and Matielli, N. (2019) Geochemistry and petrogenesis of Archean mafic rocks from the Amsaga area, West African craton, Mauritania. Precambrian Research, 324, 208-219, doi:10.1016/j.precamres.2019.02.005

Weis, D., Garcia, M. O., Rhodes, J. M., Jellinek, M., and Scoates, J. S. (2011). Role of the deep mantle in generating the compositional asymmetry of the Hawaiian mantle plume. Nature Geoscience, 4(12), 831.

Willbold, M., T. Elliott and S. Moorbath (2011) The tungsten isotopic composition of the Earth's mantle before the terminal bombardment: Nature, 477, 195-199.

Willbold, M., Mojzsis, S.J., Chen, H.-W., and Elliott, T. (2015) Tungsten isotope composition of the Acasta Gneiss Complex. Earth and Planetary Science Letters, 419, 168-177, doi:10.1016/j.epsl.2015.02.040

Workman, R.K. and S.R. Hart (2005) Major and trace element composition of the depleted MORB mantle (DMM): Earth and Planetary Science Letters, 231, 53-72.

Yamasaki, S., Kani, T., Hanan, B.B., and Tagami, T. (2009) Isotopic geochemistry of Hualalai shield-stage tholeiitic basalts from submarine North Kona region, Hawaii. Journal of Volcanology and Geochemical Research 185, 223-230, doi: 10.1016/j.volgeores.2009.06.006

Yoshino, T., Makino, Y., Suzuki, T., and Hirata, T. (2020) Grain boundary diffusion of W in lower mantle phase with implications for isotopic heterogeneity in oceanic island basalts by core-mantle interactions. Earth and Planetary Science Letters, 530, 115887, doi:10.1016/j.epsl.2019.115887

Yuan, K., and Romanowicz, B. (2017) Seismic evidence for partial melting at the root of major hot spot plumes. Science, 357, 6349, 393-397, doi:10.1126/science.aan0760